To the Graduate Council:

I am submitting herewith a thesis written by Carissa D. Snyder entitled "Metamorphic Phase Equilibria and Fluid Flow in a Contact Aureole: Tres Hermanas Mountains, Luna County, New Mexico." I have examined the electronic copy of this thesis for form and content and recommend that it be accepted in partial fulfillment of the requirements for the degree of Master of Science, with a major in Geology.

Theodore C. Labotka
Major Professor

We have read this thesis
and recommend its acceptance:

Larry Anovitz

Christopher Fedo

Accepted for Council:

Carolyn R. Hodges
Vice Provost and Dean
of the Graduate School

(Original signatures are on file with official student records.)

Metamorphic Phase Equilibria in a Contact Aureole: Tres Hermanas Mountains, Luna County, New Mexico.

A Thesis Presented for the

Master of Science

Degree

The University of Tennessee, Knoxville

Carissa D. Snyder

December 2012

DEDICATION

ACKNOWLEDGMENTS

I would like to acknowledge the Univeristy of Tennesee, the Earth and Planetary Sciences Department, and several people for helping me out and holding me up along the road to earning my Master's degree. First, I'd like to thank my advisor, Theodore "Ted" Labotka, for taking me on in unexpected circumstance, providing me with a field-based project and funding, and bearing with my persistent pestering. I would next like to acknowledge the members of my committee, Larry Anovitz and Chris Fedo, for helping with my thesis. I would like to specifically thank Larry for allowing me to use his samples. I need to thank Mike Lucas for assisting me in the field and putting up with me so well for the month long field excursion. I must thank Virginia "Ginger" McLemore for her help locating references and accompanying me in the field. She helped me become more familiar with the area and stratigraphy. I would like to thank Linda Kah and Collin Sumrall for teaching me how to make thin sections and fixing equipment problems along the way and Allan Patchen for help running the electron probe microanalyzer. I can't forget to acknowledge my fiancé, Rob Shilling, who put up with my constant frustrations along the way and was so kind as to help me in the rock room making thin sections. I also must acknowledge my family, here and gone, whose love and support pushed me through the bad times and made the good times that much better. Lastly, I need to thank my fellow graduate students, especially Ryan Roney,

Ashley Berg, Carolyn Tewksbury- Christle, Sarah Drummond, and Latisha Brengman who were always available to bounce ideas off of and to assist with editing and proofreading my thesis drafts. Thank you all so much for helping to make this possible!

ABSTRACT

To characterize the metamorphism in the Tres Hermanas Mountains contact–metamorphic aureole in Luna County, New Mexico, I mapped and collected samples of the Paleozoic strata near the quartz monzonite pluton along the northeast flank of North Peak. Stratigraphy in this area includes the Pennsylvanian undivided unit that is composed of thin-medium interbedded limestone, shale, and sandstone and the Hueco Formation that could be broken out into four members: a pebble–cobble conglomerate marks the base, a medium to massive bedded siliceous limestone is next, followed by a pure limestone member and topped by a breccia bed in places marking the fault contact with extrusive andesite. These country rocks were intruded first by andesite sills and stocks and a second time by the large quartz monzonite pluton. The metamorphic assemblages are similar for all the sedimentary rock units and include quartz, calcite, diopside, plagioclase, K-feldspar, clinozoisite, garnet, and wollastonite. Mineral composition often vary within individual samples (e.g. various compositions along the diopside-hedenbergite, grossular-andradite, and albite-anorthite solid solution series). I was able to determine that the Paleozoic stratigraphy endured a lithostatic pressure between 22.5, and 37.5 MPa, at temperatures between 245 and 505 °C, and in the presence of a very water-rich metamorphic fluid having an $X(CO_2)$ of 0.01-0.02. The previously observed high-temperature minerals were not observed in the contact aureole and may have formed as a result of the low pressure, water-rich fluids, and higher temperatures within the surrounding magma.

TABLE OF CONTENTS

LIST OF FIGURES

LIST OF TABLES

1 INTRODUCTION

This study characterizes the extent of metamorphism and fluid—rock interactions during contact metamorphism of Paleozoic carbonate strata intruded by a Tertiary quartz monzonite pluton. The study focuses on the portion of the contact aureole along the northeast face of North Peak in the Tres Hermanas Mountains of Luna County, New Mexico. Field mapping and a suite of samples from the Permian Hueco Formation and a Pennsylvanian undivided unit have been used to determine phase equilibria and fluid composition during metamorphism.

The high-temperature minerals monticellite, spurrite, and merwinite were observed by Homme (1958) in a xenolith on South Peak in the Tres Hermanas Mountains. Such high-grade minerals are unusual in contact-metamorphic aureoles. It is not the only one of its kind. Anovitz et al. (1991) observed merwinite, mellilite, rankinite, and spurrite at Marble Canyon, Texas; Burnham (1959) observed vesuvianite, monticellite, merwinite, mellilite, and spurrite in Crestmore, California; and Tracey et al. (1978) and Valleys and Essene (1980a & b) observed vesuvianite, monticellite, and akermanite at Cascade Mountain in the Adirondacks of New York. Despite several similar observations, the occurrence of these high-grade minerals is not well understood. Therefore, studies of the contact aureole and larger system are needed to understand how these minerals might have formed in the Tres Hermanas Mountains.

The occurrence of minerals thought to form at high temperature may actually be the result of low pressure metamorphism. Most reactions have a positive Claperyon slope especially if they are devolatilization reactions. The pressure of an aqueous fluid can also result in a lowering of the reaction termperature, particularly if the reaction is a decarbonation reaction. Metamorphic fluids can buffer metamorphic reactions, and rocks can record the composition and volume of the fluid. Pore fluid, meteoric fluid, and fluid released from the crystallizing pluton could have different chemical compositions and therefore, could be recognizable in the assemblage. Mixing of these fluids would have a unique signature as well. The existence of ores and veins are some of the field evidence supporting the presence of an aqueous

fluid. Understanding the mineral assemblages, textures, and reactions will help to pull apart the signatures and identify how the fluid played a part in the metamorphism.

Metamorphism at North Peak should show a progressive nature with increasing grade as you move inward toward the pluton, and the rocks may exhibit these same high-temperature minerals observed by Homme (1958) near the contact. Samples were collected along several transects moving outward from the contact to document this progressive metamorphism. Mineral assemblages were determined and used to discern the metamorphic conditions and reactions. These assemblages and mineral textures were also used to demonstrate the nature and extent of fluid—rock interaction. The primary goals of this study are 1) to identify the conditions of metamorphism, 2) to determine the nature of progressive metamorphism, and 3) to determine the nature of fluid—rock interaction within the Tres Hermanas Mountains contact-metamorphic aureole.

2 GEOLOGIC SETTING

The geology of Tres Hermanas Mountains has been previously studied by several, but the metamorphism has been largely unstudied. Investigations of the Tres Hermanas Mountains and surrounding region began with Lindgren (1909) who studiesd mineral deposits in the Tres Hermanas mining district. Darton (1916, 1917) followed with studies depicting the mineral and water resources within Luna County. Bogart (1953) investigated the upper Paleozoic stratigraphy and determined that the rocks mapped as the Gym limestone in Luna County are part of the Permian Hueco formation. Griswold (1961) described the mineral deposits. A geologic map by Balk was published posthumously in 1962 and remains the most current geologic map of the area. Kottlowski and Foster (1962) described the pre-Tertiary stratigraphy. Homme wrote a Master's thesis in 1958 on the contact metamorphism of a xenolith on South Peak (Tres Hermanas Mountains), which was published in a summary of work by Homme and Rosenzweig in 1970. Doraibue and Proctor (1972, 1973) analyzed the correlations between trace concentrations of base metals in the Tres Hermanas quartz monzonite stock and mineral deposits in the aureole. Leonard detailed the petrography of the Tres Hermanas igneous rocks in her 1982 M.S. thesis. Lance and Keller (1981) analyzed the geophysical gravity patterns in the region. Kottlowski and Armstrong (1996) described the limestone resources in the area while McLemore (1996) and McLemore et al. (2001) described the mineral resources. In 2007, Larry Anovitz (Oak Ridge National Laboratory) collected samples for his study on recrystallization (unpublished), which have been used in this study.

Homme (1958) studied the metamorphism of a xenolith along the east flank of South Peak, a mountain approximately 1.0-1.5 kilometers S45°E of the present study (Fig. 1). My study focuses on the northeast flank of North Peak. I mapped an area 6 miles north of the USA—Mexico border, at a scale of 1:12,500 encompassing approximately 1.5 mi^2 of the northeastern slopes of North Peak. The area includes sec. 25, T27S, R9W, the northern portion of sec. 36, T27S, R9W, as well as the western portion of sec. 30, T27S R8W and the northwest corner of sec. 31, T27S, R8W, all located within the North Peak quadrangle.

Deming, NM lies 30 miles to the north, and Columbus, NM is 5 miles to the southeast. The field area is managed by the Bureau of Land Management (BLM) and small private claims. The field area can be accessed by traveling New Mexico Highway 11 south from Deming and then turning west on to gated BLM roads at county road B005 Whirlwind Road.

The stratigraphy within the field area consists of Pennsylvanian and Permian near-shore to shelf facies that strike nearly due north and dip off to the east (Fig 2). Detailed descriptions of stratigraphy are given by Bogart (1953), Balk (1962), and Clemons (1998). The Hueco Formation is a fairly pure, medium- to massive-bedded, fossiliferous limestone with interbedded siltstone near the top, a few lenses of chert, and rare chert nodules. The Pennsylvanian undivided unit is thin- to medium-bedded limestone, shale, and a few sandstone layers. Fossils are rare, but chert nodules are prevalent. I collected samples from the contact with the quartz monzonite and in both units along several transects. Intense metamorphism as indicated by wollastionite, skarn layers, local deformation, and sometimes coarse recrystallized limestone, is more evident in the Pennsylvanian undivided.

The Tres Hermanas Mountains are part of a volcanic terrane created by extensional magmatism associated with the opening of the Rio Grande Rift and Basin and Range orogenic event. This terrane stretches across portions of northern Mexico, Texas, New Mexico, Arizona, and Colorado. The igneous rocks in the Tres Hermanas Mountains are part of the Boot Heel volcanic field within this larger terrane (Chapin et al., 2004). A quartz monzonite pluton that is roughly circular in shape and covers approximately 10 square kilometers makes up the bulk of the Tres Hermanas Mountains. The margins of the pluton are nearly vertical with contacts that dip approximately 70° to the east. The Paleozoic strata intruded by the quartz monzonite strike nearly due north and dip off to the east at approximately 35°. The quartz monzonite contact is usually covered by boulders and colluvium. Blocks of country rock with assimilation-like textures can be observed within the quartz monzonite. The sedimentary stratigraphy is metamorphosed along the country rock but doesn't appear to differ in texture, composition, or structure with proximity to the contact. The outer limit of the contact aureole was not observed and may be

obscured by Cenozoic alluvial deposits. Several quartz monzonite dikes and apophyses cross-cut the sedimentary rocks. Jasper dikes are often observed adjacent to quartz monzonite dikes (Fig 3). McLemore et al. (2001) reported an ^{35}Ar-^{40}Ar date on hornblende in the quartz monzonite as 34.65 ± 0.28 Ma.

Andesite intrudes the Palezoic strata in the Tres Hermanas Mountains as well. Vertical intrusions create a large portion of three adjacent ridges in the field area, and sills are observed connecting them in the stream valleys. Andesite dikes are also present. Quartz monzonite cross-cuts the andesite, but intrusive andesite is never observed cross-cutting the quartz monzonite. McLemore (personal commun. 2012) is measuring the age of the andesite.

The oldest rocks in the field area are the Permian Hueco Formation and the Pennsylvanian undivided unit. These sedimentary rocks were altered to marble, calc-silicate rock, and other siliceous rock. Four members could be separated from the Hueco Formation. At the base is a reddish-purple pebble—cobble conglomerate member with interbedded black siliceous layers totaling approximately 50 feet in thickness. Above that is the olive-green to tan middle limestone member, which is medium- to massive-bedded, microcrystalline limestone with siliceous lenses throughout and chert-pebble conglomerate lenses near the bottom. The gray upper limestone member is a massive-bedded, fossiliferous cryptocrystalline, pure limestone with rare chert nodules. A breccia bed could be mapped as a separate member in places at the top of the Hueco sequence, which marks a fault contact. The Pennsylvanian undivided unit is considerably different with thinly interbedded limestone, shale, and sandstone. The limestone is similar to that of the upper gray limestone member of the Hueco Formation but contains fewer fossils and more abundant chert nodules. The northern-most ridge in the study area is capped by a massive sandstone bed. Fossil assemblages within the two formations are markedly different as well. Fossils in the Hueco are predominantly gastropod fauna, while those in the Pennsylvanian undivided are primarily crinoids.

Intense metamorphism, noted by deformation and large metamorphic minerals (e.g. wollastonite, garnet, and diopside) (Fig 4), is evident in Pennsylvanian rocks near vertical intrusions of andesite but is minimal

with no marked effects near sills and dikes. An increased grain size in the recrystallized limestone was also observed near some vertical andesite intrusions. Altered andesite was observed near quartz monzonite intrusions. Wholesale metamorphism was evident near quartz monzonite contacts, but textural differences such as an increasing metamorphic grade, deformation, or grain size, were not evident. Several veins, weathered brecciated pockets (Fig 5), yellow-green clay alteration zones, and ore bodies are evidence for the existence of an aqueous fluid within the aureole.

3 METHODS

Sedimentary rocks are exposed in incised stream valleys and along ridge spurs. Sampling stations care shown in Figure 6. Samples were collected along transects when a change in rock type was observed or a marked difference in composition or texture occurred within a rock type. The fine-grained nature of those samples made mineral identification difficult. Therefore, X-ray diffraction (XRD) analyses were conducted on thin sections. Individual analyses were completed from 5° through 70° at 0.02° increments. The voltage was set at 40kV and the current at 30mA. Crystal Maker and PDXL programs were used to identify peaks and match to minerals. An example is shown in Figure 7. This method assumes the x-rayed area is homogenous and includes all phases. Therefore, some minerals may have been missed. Mineral identification was refined in some cases by thin section observation. Eleven samples were selected for additional analysis with the electron probe microanalyzer (EPMA). Point analyses and x-ray images were obtained using a CAMECA SX-100 fully-automated electron probe microanalyzer. An acceleration voltage of 15 kV, a beam current of 20 nA, a spot size of 1 μm, and a 20 s count time were used for most point analyses. Feldspar, scapolite, and zeolite minerals were analyzed with a current of 10 nA and a spot size of 10 μm. Natural and synthetic standards were checked before and after each use of the EPMA and both the PAP (Pouchou and Pichoir 1985) procedure and matrix corrections (atomic number, absorption, and fluorescence) were applied. Detection limits of 0.03 weight percent were used for all elements except Fe and Mg, which had detection limits of 0.05 weight percent. Several X-ray images of Ca, Mg, Al, Si, Fe, K, Cl, and Ti, were made with a count time of 50 ms and a step size of 1-7 μm. Estimated pressure and Powell and Holland (1988) datasets were used to construct T-X(CO_2) diagrams in THERMOCALC (White et al., 2007). Table 1 lists the assemblages observed in these 11 samples (assemblages of all analyzed samples can be found in the appendix). Representative analyses are included in Tables 4 through 8 and full analyses can be found in the appendix.

4 PHASE EQUILIBRIA

4.1 MINERAL ASSEMBLAGES

In a carbonate contact aureole, assemblages are predicted to contain a subset of the minerals in Figure 8 and to be produced through progressive metamorphic reactions outlined in Figure 9 (refer to Table 2 for nomenclature descriptions). The specific reactions and resultant assemblages change with any variation in pressure, temperature, or fluxuations in the quantity or composition of fluid present. Considering the metamorphic reactions in Table 3 for a siliceous limestone, the metamorphic assemblages may include 1) the minerals present in the reactants or products for a given metamorphic reaction, 2) a mixture of minerals from reactants or products when multiple metamorphic reactions co-occur or 3) all the minerals in the reactants and products for a given metamorphic reaction (with additional minerals possible from the reactants or products of additional reactions). The first two examples could represent equilibrium assemblages, while the third might not represent equilibrium. Diffusion of heat from the pluton into the country rocks should produce higher-temperature assemblages near the contact and should decrease in grade as you move away.

Samples were analyzed from the Hueco gray upper limestone and olive-green middle limestone members and from the Pennsylvanian undivided unit. Assemblages in the Hueco Formation vary only slightly from those observed in the Pennsylvanian undivided unit. Maps demonstrating the spatial distribution of the assemblages are shown in Figure 10. Low-grade and high-grade assemblages are intermingled and some samples have assemblages containing all the minerals involved in a single metamorphic reaction. Characteristics of each member of the Hueco Formation and the Pennsylvanian undivided unit are described below.

The Hueco gray upper limestone member is the purest carbonate protolith. The assemblage in this rock is calcite + K-feldspar + diopside + garnet + clinozoisite. Quartz, plagioclase, and an

unidentified zeolite were also observed in some samples (Table 1). XRD analyses indicated the presence of forsterite in several samples, but may have been misidentified since it was not observed in thin section or EPMA analysis. Wollastonite was also indicated by XRD but not verified with additional analyses. Some portions of this member exhibited bleaching of the limestone, or silicification (Figs 11 and 12).

The Hueco olive-green middle limestone member is more siliceous than the upper member. The assemblage in this rock type is calcite + plagioclase + K-feldspar + diopside + garnet + clinozoisite. Wollastonite, quartz, scapolite, and an unidentified zeolite were observed in some samples (Table 1). Forsterite was indicated by XRD analysis of this rock type as well, but has not been verified. This member was observed in the field with many characteristics of metamorphism including mottled textures, several varieties of porphyroblasts (diopside, garnet, and wollastonite), and significant veining in places. The alteration of this member was the most significant and varied in the field.

The Pennsylvanian undivided unit has the most silica content because of the interbedded shale and sandstone. However, calcite in the limestone and shale is still the dominant mineral. The assemblage in this unit is diopside + garnet + wollastonite. Calcite, quartz, plagioclase, K-feldspar, scapolite, and clinozoisite were also observed in some samples (Table 1). Wollastonite was observed in samples far from the quartz monzonite contact in the northern portion of the field area (Fig 10C). Skarn layers, several centimeters thick, were observed within this unit. Sandstone beds were recrystallized to quartzite.

4.2 MINERAL COMPOSITIONS

Pyroxene is observed in most samples. Diopside is the most common porphyroblast (Fig. 13) ranging in size from a few tens of micrometers to a few centimeters in length. Grains are usually anhedral with reaction textures especially near the edges. Inclusions are common and may consist of sphene (most common), garnet, or pyrite (very large in some samples). The diopside has a range in

composition along the diopside-hedenbergite solid solution series with hedenbergite contents from 0 to 70%. In addition to Ca, Mg, Fe, and Si, these clinopyroxene grains have 0-6% Al_2O_3 and trace quantities of Mn and Ti. Some diopside porphyroblasts exhibit heterogeneous zonation of Fe and Mg compositions (Fig 13B). Representative analyses are provided in Table 4, and compositions are plotted in Figure 14. Samples TH12S-074, -094, -100, and -116 cluster along the diopside-hedenbergite solid-solution line between 0 and 20% hedenbergite. Sample TH12S-176C clusters with a range in hedenbergite content between 0 and 30%. Samples TH12S-102, -110, and -112 cluster between hedenbergite contents of 20 to 40%. Sample TH12S-131 demonstrates a range in hedenbergite content between 30 and 62% while sample TH07A-4 demonstrates a range between 20 and 67%.

Wollastonite occurs as anhedral grains and fanning bundles of euhedral laths that range in size from a few tens of micrometers to several centimeters. Reaction textures are often observed in anhedral grains and reaction pockets are observed inside the edges of grains in some samples (Fig 15). Wollastonite compositions are pure $CaSiO_3$. Representative analyses are provided in Table 4, and compositions are plotted in Figure 14. Wollastonite is found in samples TH12S-074, -102, and -112. These samples contain diopside grains as well with compositions that range in hedenbergite content between 0 and 40%. No pyroxene or wollastonite was observed in sample TH12S-155, which is a pure calcite limestone containing chert nodules.

Garnet is the dominant phase in some samples and is the second most common porphyroblast. Garnet grains are anhedral to euhedral and range from a few tens to several hundred micrometers in size. Some grains exhibit growth rings while other samples exhibit reaction textures especially near the edges. Cracks filled with calcite, quartz, or feldspar are observed in garnet from some samples. Compositions range between grossular and andradite. Compositional zonations involving Fe and Al are observed within some grains, as demonstrated in Figure 16. These variations usually occur in growth rings and rims. Representative analyses are shown in Table 5, and the observed compositions

are plotted in Figure 17. Most garnet analyses are 70-85% grossular, and only a few samples exhibit more of an andradite composition ranging between 15-30% grossular. One sample in particular (TH12S-074) shown in Figure 16A is classified as a skarn, and is composed primarily of andradite.

Plagioclase and K-feldspar are observed in several samples. The K-feldspar is composed of K, Al, Si, 0.4-1 weight % Na_2O, 0-2 weight % BaO, and trace concentrations of Mg, Ca, and Fe. It occurs as anhedral grains and intergranular matrix ranging from a few tens of micrometers to a couple hundred micrometers in size. The K-feldspar is usually observed in association with pyroxene. Plagioclase also occurs as anhedral grains and as intergranular matrix ranging from a few tens of micrometers to a couple hundred micrometers in size. The composition of plagioclase runs the full range in solid solution. Trace amounts of Mg, Fe, and K are also observed. Weight percent and cation totals are very close to expected values, so it is not likely that other elements, not analyzed in this study, are included in the chemical composition. Representative analyses are provided in Table 6, and compositions are plotted in Figure 18. Two samples, TH12S-100 and -102, have assemblages with K-feldspar but no plagioclase. Sample TH12S-176C contains plagioclase with a range in anorthite content of 5-100% but does not contain K-feldspar. Samples TH12S-116, -094, and TH07A-4 have assemblages with K-feldspar that also contain plagioclase with a range in anorthite content of 0-25%. Sample TH12S-131 has an assemblage with K-feldspar that also has plagioclase with a range in anorthite content of 0-58%. Sample TH12S-112 has an assemblage with K-feldspar that also contains plagioclase with a range in anorthite content of 55-88%. Sample TH12S-110 has an assemblage with K-feldspar that includes plagioclase with a range in anorthite content between 45 and 72%. Two of the samples studied with EPMA analyses do not contain feldspar; TH12S-074 is a skarn and TH12S-155 is a pure calcite limestone with chert nodules. Both of these samples occur in the Pennsylvanian undivided unit.

Scapolite was observed in two samples. The grains are usually anhedral and reach as much as a few tens of micrometers in length. Scapolite is usually found in association with another Na-bearing

mineral such as albite or zeolite (Fig 15). The Na:Ca ratio of scapolite, plagioclase and zeolite in these assemblages are 2.45, 3.57, and 0.55 respectively. The composition includes a chlorine component but does not fall as end-member marialite as shown in Figure 19. Representative analyses are given in Table 7.

Epidote is observed in several samples as grains and vein fill. Grains are typically anhedral and range in size from a few tens to a few hundred micrometers. Most analyses indicated a clinozoisite composition, but one sample had REE such as Ce and La, which indicated allanite compositions. Representative analyses are given in Table 8. The clinozoisite composition varied with a range of 4-14% Fe_2O_3, and trace quantities of Ti, Mg, and Mn.

Calcite occurs as veins, grains, and as intergranular masses. The grains typically range from anhedral to euhedral and are a few tens to a few hundred micrometers in size. Fossils are most often preserved by calcite. Detailed compositional anyalses were not conducted on calcite due to devolitilization by the electron beam.

Quartz occurs throughout the aureole as veins, grains a few tens of micrometers in size, and as intergranular mass. Chert nodules occur in the original rock types, and some have been preserved during metamorphism. Others have been replaced, and are now pyroxene + feldspar assemblages. Quartz occasionally exhibits undulose extinction and may exhibit 120° grain boundaries. Some fossils are preserved by quartz. Most pebbles in conglomerate beds and lenses were originally limestone, and have been at least partially altered to quartz. Several orange-brown jasper dikes (Fig 3) are observed across the aureole. These dikes are often found adjacent to quartz monzonite dikes. Large quartz veins are often found near mine pits or shafts.

4.3 REACTIONS AND ISOGRADS

The reactions that seem to be the most important for the observed assemblages include those that formed the minerals diopside, garnet, and wollastonite, and any reactions that occurred between these minerals. Table 3 lists the reactions that are likely to be involved in progressive metamorphism of the Tres Hermanas Mountains. Reactions 4, 5, and 7 produce diopside, garnet, and wollastonite respectively. Reaction 11 demonstrates an additional relationship between garnet and wollastonite.

Figure 10 displays the spatial distribution of observed assemblages involving the metamorphic minerals diopside, garnet, and wollastonite. The garnet and wollastonite maps were compiled using assemblages on either side of reactions 5, 7, and 11 in Table 3. The minerals on the low temperature sides of diopside-forming reactions are not present or may need additional analyses to determine their full extent. Therefore, the diopside assemblage map is not compiled using specific reactions. Instead, this map marks the distribution of diopside, garnet and wollastonite simultaneously, which indicates various ranges in temperature. Garnet forms at a higher temperature than diopside and the wollastonite-forming temperature is higher yet according to Figure 9.

A simple temperature gradient with high-grade assemblages near the contact and assemblages of decreasing grade moving outwards is not shown in Figure 10. This is not typical of the hypothesized single progressive metamorphic event. High-temperature assemblages are observed intermingled among low-temperature assemblages. The random mixture of different grades does not appear to produce any other patterns. Some samples encompass all minerals involved in reactions such as cc + qtz + wol, cc + qtz + an + gr, and gr + qtz + an + wol (reactions 5,7, and 11 from Table 3). It would be ideal to use the reactions that produce the key metamorphic minerals, diopside, garnet, and wollastonite, to identify isograds. However, without patterns in the occurrence of these minerals or assemblages, no isograds can be drawn.

Several textures are observed in samples from the contact aureole. Porphyroblasts of diopside, wollastonite, or garnet (Figs 13, 15, and 16) are prevalent. In thin section, most of these porphyroblasts demonstrate a reaction texture around the edges. Some slides exhibit this reaction texture in all phases. Reaction rims are visible around some porphyroblasts such as the diopside seen in Figure 13B. The edge of the diopside is manteled by a ring of plagioclase, an outer ring of diopside, and then a ring of K-feldspar + plagioclase as you move outward from the intact porphyroblast. Porphyroblasts and reaction rims or patches can produce mottled textures in hand samples. Veining is prevalent in some areas as well. These veins are primarily composed of calcite, quartz, or epidote. An epidote vein is shown in Figure 13B. Some veins also demonstrate reaction rims. Grain size within the aureole is typically very fine, but some areas contain recrystallized limestone with calcite grains a few centimeters in size (Fig 20). While some textures are observed over several centimeters to meters in outcrop, most reaction textures occur in localized areas a few tens to hundreds of micrometers in diameter, and indicate local phase equilibrium.

A few observations suggest metasomatism may have participated in the metamorphism of the Tres Hermanas Mountains. The presence of large jasper dikes (Fig 3) suggests that siliceous fluids flowed through the aureole. Silicification of limestone seen in Figure 12 and limestone pebbles partially or entirely converted to quartz suggests a silica-rich fluid interacted with the rocks to replace calcite with quartz. The bleaching of limestone observed in Figure 11 is also attributed to fluid—rock interaction. Some chert nodules were observed to have been replaced by pyroxene + feldspar assemblages (Fig 21). This is likely due to interaction with fluids as well. The abundance of silica and possibly other elements in the metamorphic asssemblages are greater than what is expected for the limestone protolith. Metasomatic fluids can act as a transport medium for silica and other elements and may be responsible for the elevated concentrations. The heterogenous zonations of hedenbergite and diopside in Figure 13B is a odd occurrence that may only be explained by incongruent interaction with a fluid on a scale of hundreds of micrometers or less. This evidence suggests metasomatism is a likely

process contributing to the metamorphic assemblages and producing some of the reaction textures and anomalous assemblages observed throughout the aureole.

5 CONDITIONS OF METAMORPHISM

The pressure during metamorphism can be estimated by the lithostatic stress induced by overburden during the time of intrusion. The stratigraphic thickness for Paleozoic and pre-intrusion Cenozoic sediments was compiled from the work of Griswold (1961), Balk (1962), and Leonard (1982) (Table 9). The estimated overburden ranges between 0.85 and 1.4 kilometers, which corresponds to a lithostatic stress between 22.5 and 37.1 MPa respectively. Miarolitic textures observed in the quartz monzonite indicate low pressure, and typically form in magma chambers with pressure less than 250 MPa (Candela and Blevins, 1995). The lithostatic pressure falls well within the upper limit set by miarolitic textures.

Temperature may be dispersed in two ways – conduction and convection – which are recorded in the metamorphic assemblages by specific signatures. High-temperature mineral assemblages near the contact and low-temperature mineral assemblages farther away are produced by conduction of heat from the pluton outward into the country rocks. Convection of heat by fluid in the aureole can produce high-temperature assemblages along flow paths. Circulatory flow paths, as opposed to linear flow paths, could allow warm water to be circulated, heated again, and percolate through the system repeatedly producing anomalous patterns of metamorphic assemlages throughout the aureole. It is unclear from this dataset how fluids flowed in the contact aureole because there does not seem to be a pattern to the occurrence of high-grade assemblages.

A range in temperature for metamorphism is determined by assemblages related to the formation of key metamorphic minerals outlined in Figures 8 and 9. THERMOCALC (White et al., 2007) was used to calculate T-X(CO_2) diagrams (Figs 22-23) at a pressure of 22.5 MPa. According to these calculations and depending on X(CO_2) in the metamorphic fluid, diopside forms between 265 and 385 °C, garnet between 245 and 430 °C, wollastonite between 295 and 450 °C, and forsterite between 330 and 450 °C. Wollastonite may also form by a fluid-independent reaction at or above 498 °C. Depending on the assemblage, the temperature during metamorphism is somewhere in the range of 245-498 °C. Monticellite

forms above 650 °C, but it is absent in the contact aureole. Therefore, the upper limit must be below this temperature. The variation in estimated pressure due to lithostatic stress has an effect on the possible temperature, which results in an elevated range in temperature of 260-505 °C at 37.5 MPa.

Evidence of fluid—rock interaction observed in the lab includes a prevalence of reaction textures and a higher concentration of elements (e.g. Na, Mg, Cl, etc.) in metamorphic assemblages than were present in the original rock. THERMOCALC calculations for the reaction

$$3\ an + cc \leftrightarrow 2\ zo + CO_2$$

was used to determine the fugacity ratio of CO_2 and H_2O in the metamorphic fluids present during the formation of zoisite. THERMOCALC was used to calculate an equilibrium constant (K_{eq}) for the zoisite-forming reaction of 9.31 given a range in temperature of 100–700 °C and a pressure of 30.0 MPa (linearized at 400 °C). Using the equation for the equilibrium constant,

$$K_{eq} = [X(Al)^6 * f(CO_2)]/[X(Ca)^3 * f(H_2O)]$$

$$K_{eq} = \frac{X_{Al}^6 \, x \, f_{CO2}}{X_{Ca}^2 \, x \, f_{H2O}}$$

where X(Al) is the mole fraction of aluminum in clinozoisite, X(Ca) is the mole fraction of calcium in the plagioclase, and *f* is fugacity. Rearranging this equation allows you to solve for the fugacity ratio as follows

$$\frac{f_{\mathrm{H2O}}}{f_{CO2}} = Keq \; x \; \frac{\mathrm{X}_{Al}^6}{\mathrm{X}_{Ca}^2}$$

Mole fractions derived from the EPMA analyses of plagioclase and clinozoisite in sample TH12S-131 were used to determine a H_2O/CO_2 fugacity ratio of 500. Assuming total pressure is the sum of only water vapor pressure and carbon dioxide vapor pressure, a line (shown in red) can be plotted on Figure 24 that

intersects the ideal fluid curve [constructed using f(CO_2) data from Span and Wagner (1996), f(H_2O) data from Wagner and Pruss (1993), and CO_2—H_2O activity data from Blencoe et al. (2001)] shown in blue . The intersection of these two lines indicates the X(CO_2) is between 0.01 and 0.02. This has several implications for understanding the physical conditions during metamorphism. Increased water content allows high-grade minerals to form at a low temperature. In Figures 22 and 23, an X(CO_2) of 0.01-0.02 at 400 degrees, occurs very close to the y-axis and allows for wollastonite-grade assemblages to form. The temperature range based on the formation of assemblage minerals at the determined X(CO2) is 317-390 °C at 22.5 MPa unless wollastonite is being formed by the second reaction at 498 °C (333-401 °C and second wollastonite reaction at 505 °C at 37.5 MPa). Vesuvianite might be expected to form in this fluid composition, but it did not (Fig 23). The mineral sequence and thus metamorphic grades are also affected by such a water-rich fluid. In this region of curve 3 (Fig 23), garnet forms at a temperature less than or equal to that necessary to form diopside (see Fig 23 inset). The mineral assemblages and compositions indicate the T-X conditions to be in the red shaded region which allows for the formation of diopside, garnet, and wollastonite between the temperature of 245 and 498 °C.

6 DISCUSSION

The original siliceous limestones are suitable for forming all the metamorphic minerals in Figure 8 given the necessary temperatures are sustained. The absence of talc and the rarity of tremolite may be a result of consumption in subsequent reactions. Diopside was most likely formed by the reaction

$$3\ cc + 2\ qtz + tr \leftrightarrow 5\ di + 3\ CO_2 + 2\ H_2O$$

but may have formed by the reaction

$$phl + 6\ qtz + 3\ cc \leftrightarrow ksp + 3\ di + 3\ CO_2 + H_2O$$

if phlogopite was once more abundant. Garnet was formed by a reaction involving calcite, quartz, and anorthite. The lack of dolomite suggests that if forsterite is present, it most likely formed by the reaction

$$5\ cc + 3\ tr \leftrightarrow 11\ di + 2\ fo + 5\ CO_2 + 3\ H_2O.$$

Given the present assemblages, wollastonite may have formed by both fluid-dependent and fluid-independent reactions. At a pressure of 22.5 MPa and a temperature high enough to form wollastonite, vesuvianite is expected to form in a temperature range of 235-395 °C and $X(CO_2)$ between 0 and 0.1. The absence of vesuvianite may be a result of the quantity of reactants needed and their consumption in other reactions limiting the availability to the vesuvianite-forming reactions. If reactant availability is adequate, then fluid compositions too rich in CO_2 may have prohibited the formation of vesuvianite.

Some assemblages contain sll the reactant and product minerals for some metamorphic reactions. This anomaly could be evidence of solid solution or retrogradation and may be supported by the reaction textures in all phases in the assemblage. It is more likely that fluid–rock interaction affected portions of the rock differentlyas a result of variations in porosity or mineral compositions. Further evidence for fluid–rock interaction comes from the equilibrium on scales of a few centimeters or less, as indicated by the different assemblages within a single stratigraphic unit, large compositional variations witihin

pyroxene, garnet, and plagioclase within a single thin section, and corona-like textures shown in Fig 13B. The appearance of wollastonite so far from the quartz monzonite contact and in proximity to intrusive andesite in the northern portion of the field area may indicate that rocks were metamorphosed by the andesite first and overprinted by the intrusion of quartz monzonite. The observation of intense metamorphism in proximity to vertical andesite intrusions also supports this claim. However, both observations could also have resulted from preferential fluid pathways dispersing heat and fluid to these areas.

Homme's (1958) observation of high temperature minerals in a xenolith on South Peak seems anomalous for this relatively low-temperature system. The contact aureole would not reach exactly the same temperature of the magma during metamorphism, but a carbonate block immersed in the magma is likely to endure at least slightly higher temperature than the contact aureole. In addition, fluid in the magma is likely to have been H_2O-rich, which coul reduce the necessary temperature required to produce the high-temperature mineral assemblage. Therefore it is reasonable that a xenolith would contain the observed high-temperature minerals not observed in the contact aureole. Simple heat-flow calculations are often used to describe the heat available to produce progressive metamorphism. Heat flow appears to be complex in the Tres Hermanas Mountains, since progressive metamorphic zones are not found in the aureole. The high-temperature mineral wollastonite being observed considerably far from the contact also supports a complex heat and fluid flow system.

Metamorphism in a carbonate contact aureole is produced through a series of decarbonation Metamorphic fluid is composed of pore fluid and CO_2 produced by the reactions. The $X(CO_2)$ of 0.01—0.02 calculated for the contact aureole is very water-rich. The CO_2 must have been removed or diluted to produce such a composition. Because of the shallowness in the Earth's crust during pluton emplacement, it is likely that some CO_2 escaped through fractures or fissures. At this temperature and pressure, H_2O and CO_2 fluid could develop immiscibility (Labotka, 1991). A less dense CO_2-rich fluid is more likely to move upward and escape the system leaving behind a more H_2O-rich fluid. Felsic plutons are often quite

water-rich and release those aqueous fluids during crystallization. It could be that an H_2O-rich fluid flushed through the system continuously enough to dilute the CO_2 to produce this composition. At merely a kilometer deep in the crust, meteoric waters are also possible and could have diluted metamorphic fluids.

An approximation of how much water is required to dilute a pure CO_2 fluid to $X(CO_2)$ calculated for the Tres Hermanas contact aureole can be done with a mass balance calculation according to the reaction,

$$3\ an + cc + H_2O \leftrightarrow 2\ czo + CO_2.$$

Assuming a stoichiometric mixture of anorthite and calcite, these moles of anorthite exist to every mole of calcite. Using the gram formula units, a rock with this exact ratio would weigh 931.67 grams (3moles An x 277.2g/mol An + 1 mole Cc x 100.07g/mol Cc). To consider a 1 kg sample of rock, multiply by a factor of 1.07 :3 mol An x 1.07 = 3.21 mol An, and 1 mol Cc x 1.07 = 1.07 mol Cc). One kg of rock would produce 1.07 mol CO_2 and 2.14 mol of clinozoisite for every mole of H_2O consumed during reaction. The amount of H_2O needed to produce an $X(CO_2)$ of 0.01 from mineral equilibria, is calculated with the following equation:

$$X_{CO2} = \frac{\nu_{CO2} \text{ x } \xi}{(\nu_{CO2} + \nu_{H2O}) \text{ x } \xi + n^i_{H2O}}$$

X(CO2) is the mole fraction of carbon dioxide in fluid, ν is the stoichiometric coefficient, ξ is the extent of reaction, and $n_{H2O}{}^i$ is the moles of H_2O infiltrated. The extent of reaction is calculated by $\xi = (n_i - n_i{}^0) / \nu_i$, where n_i is the moles of a mineral (final minus initial) and ν_i is the stoichiometric coeffiecient of a component in the mineral. Substituting in values of $\xi = 1.07$, $\nu_{CO2} = 1$, and $\nu_{H2O} = -1$ and rearranging to solve for $n_{H2O}{}^i$ gives the equation:$n_{H2O}{}^i = \xi / X(CO_2) = 1.07/0.01 = 107$ mol/kg = 1.926

$$n^i_{H2O} = \frac{\xi}{X_{CO2}} = \frac{1.07}{0.01} = 107 \text{ mol/kg} = 1.926$$

The volumetric fluid:rock ratio was calculated using a density of H_2O of 0.358 g/cm^3 at 400 °C and 30.0 MPa (Marin et al., 2006).

$$1.926\ kg\ \text{x}\ \frac{1000\ g}{1\ kg}\ x\ \frac{1 cu.cm}{0.358\ g} = 5379.89\ cu.cm$$

$$\frac{0.01\ l}{1\ cu.cm} = 5.38\ l$$

$$\frac{5379.89\ cu.cm\ H2O}{365\ cu.cm\ rock} = 14.7$$

A kilogram of this rock is 365 cm^3: [(3.21mol An x 277.2 g/mol)/2.73 g/cm^3] + [(1.07 mol Cc x 100.07 g/mol)/2.71 g/cm^3] = 365 cm^3. Therefore, 5.38 liters of H_2O are required per 365 cm^3 of rock to produce a X(CO_2) of 0.01. The calculated ratio of 14.7:1 is a large ratio and requires a lot of water; more than what exists as pore fluid alone. Therefore, additional water had to have been added. This excess fluid must have been produced by the pluton or the meteoric system in this shallow environment.

Evidence of metasomatic alteration has been observed in the Tres Hermanas aureole and may have produced some of the anomalies in the metamorphic assemblages. Metamorphism changes the bulk assemblages by reacting what is available in the protolith. Metamorphic assemblages in a carbonate aureole should contain Ca, Si, Mg, etc. in concentrations similar to those observed in the protolith. Metasomatism could introduce new elements during metamorphism that would produce new and unexpected minerals. Metasomatism can also bring in more of a present element such as Si to produce an assemblage with concentrations of elements that do not reflect those of the protolith. The Hueco Formation is a fairly pure calcite limestone with minor amounts of chert and should therefore contain abundant Ca, C, and O; minor Si; and traces of Mn, Mg, Fe, and Na from clay minerals. A quick bulk composition calculation of the matrix in sample TH12S-112 (Table 10; see Appendix 6 for the full calculation) demonstrates elevated values of Si and Al. Mg may also be elevated depending on the dolomite, and clay content of the protolith. No data is currently available to compare these values to

unaltered Hueco Formation. However, when compared to Labotka et al. (1988), this sample plots in the realm of an argillite (Fig, 25). Bulk composition analyses of additional samples may support mobilization of other elements. Metasomatic alterations of this kind are dependent on infiltration of fluid and therefore may be limited to small areas where porosity and permeability allowed for the movement and introduction of fluid. Chert nodules are typically composed of quartz with only trace amounts of other elements. Observations of "chert" nodules now composed of pyroxene and feldspar indicates that metasomatism with fluids enriched in Mg, K, Fe. was at least partially responsible for the present metamorphic assemblages. The apparent change in bulk composition may have resulted from the large fluid—rock ratio indicated by the assemblages.

7 CONCLUSIONS

Contact metamorphism of Paleozoic sedimentary rocks is observed in the Tres Hermanas Mountains. High-grade metamorphism was produced by low temperature, low pressure, and H_2O-rich metamorphic fluids. CO_2 produced by the decarbonation reactions probably escaped through fractures in the shallow environment and became diluted by aqueous fluids released from the cooling pluton. The metamorphic signature is complicated by overprinting of multiple metamorphic episodes and a possible hydrothermal system. Rock types are not significantly different between units and therefore, do not produce a large difference in metamorphic assemblages or style of metamorphism.

REFERENCES

Anovitz, L.M., Kalin, R.M., and Ruiz, J., 1991, High temperature contact metamorphism: Marble Canyon, West Texas: *in* Geological Society of America Abstracts with Programs, 23.

Balk, R., 1961, Geologic map and sections of Tres Hermanas Mountains: New Mexico Bureau Mines and Mineral Resources Geologic Map 16.

Blencoe, J.G., Anovitz, L.M., Singh, J., Seitz, J.C., 2001, Relative buoyancies of CO_2-H_2O mixtures at 300-400 degrees C and pressures to 100 megapascals *in* Geological Society of America Abstracts with Programs, 33, p. A17.

Bogart, L.E., 1953, The Hueco (Gym) limestone, Luna County, New Mexico: University of New Mexico unpublished master's thesis, 91 p.

Burnham, C.W., 1959, Contact metamorphism of magnesian limestones at Crestmore, California: *in* Geological Society of America Bulletin, 70, p. 879-920.

Candela, P. A. and Blevin, P. L., 1995. Do some miarolitic granites preserve evidence of magmatic volatile phase permeability? *in* Economic Geology, 90, p. 2310–2316.

Chapin, C.E., McIntosh, W.C., and Chamberlin, R.M., 2004, The late Eocene-Oligocene peak of Cenozoic volcanism in southwestern New Mexico: *in* Mack, G.H. and Giles, K.A., eds., The Geology of New Mexico: A Geologic History: New Mexico Geological Society Special Publication 11, 474 p.

Clemons, R.E., 1998, Geology of the Florida Mountains, Luna County, New Mexico: New Mexico Bureau of Mines and Mineral Resources, Memoir 43.

Griswold, G.B., 1961, Mineral deposits of Luna County, New Mexico: New Mexico Bureau of Mines and Mineral Resources Bulletin 72, 157 p.

Heinrich, W., 2007, Fluid immiscibility in metamorphic rocks: Reviews in Mineraology and Geochemistry, 65, p. 389-430.

Homme, F.C., 1958, Contact Metamorphism in the Tres Hermanas Mountains, Luna County, New Mexico: Univ. of New Mexico unpublished master's thesis, 88 p.

Labotka, T.C., 1991, Chemical and physical properties of fluids: *in* Kerrick, D.M., eds., Reviews in Mineralogy – Contact Metamorphism, 26, 847 p.

Labotka, T.C., Nabelek, P.I., Papike, J.J., Hover-Granath, V.C., and Laul, J.C., 1988, Effects of contact metamorphism on the chemistry of calcareous rocks in the Big Horse Limestone Member, Notch Peak, Utah, *in* American Mineralogist, 73, p. 1095-1110.

Leonard, M.L., 1982, The geology of the Tres Hermanas Mountains, Luna County, New Mexico: University of Texas master's thesis, 105 p.

Marin, T.W., Takahashi, K., and Bartels, D.M., 2006, Temperature and density dependence of the light and heavy water ultraviolet absortion edge: *in* the Journal of Chemical Physics. V. 125, 10, 11 p.

McLemore, V.T., Donahue, K., Breese, M., Jackson, M.L., Arbuckle, J., and Jones, G., 2001, Mineral-resource assessment of Luna County, New Mexico: New Mexico Bureau of Geology and Mineral Resources Open-file Report OF-459, Socorro, New Mexico.

Pouchou, J.L., and Pichoir, F., 1985, "PAP" *(φ-ρ-Z)* correction procedure for improved quantitative microanalysis. In J.T. Armstrong, Ed., Microbeam analysis, p. 104-106. San Francisco Press, California.

Span, R., and Wagner, W., 1996, A new equation of state for carbon dioxide covering the fluid region from the triple-point temperature to 1100K at pressures up to 800 MPa *in* Journal of Physical and Chemical Reference Data, 25, p. 1509-1596.

Tracey, R.J., Jaffe, H.W., and Robinson, Peter, 1978, Monticellite marble as Cascade Mountain, Adirondack Mountains, New York: *in* American Mineralogist, 63, p. 991-999.

USGS, 1965, North Peak Quadrangle, Luna County, New Mexico, 7.5 Minute Series, Topographic, 1:24000, 1 sheet.

Valley, J.W., and Essene, E.J., 1980a, Akermanite in the Cascade Slide xenolith, and its significance for regional metamorphism in the Adirondacks: *in* Contributions to Mineralogy and Petrology, 74, p. 143-152.

Valley, J.W., and Essene, E.J., 1980b, Calc-silicate reactions in Adirondack marble: The role of fluids and solid solution: *in* Geological Society of America Bulletin, 91, p. 114-117, 720-815.

Wagner W, and Pruss A (1993) International equations for the saturation properties of ordinary water substance. Revised according to the international temperature scale of 1990. J Phys Chem Ref Data 22:783–788Powell, R. & Holland, T. J. B., 1988. An internally consistent thermodynamic dataset with uncertainties and correlations: 3. Application methods, worked examples and a computer program. Journal of Metamorphic Geology, 6, p. 173–204.

White, R.W., Powell, R., and Holland, T.J.B., 2007, Progress relating to calculation of partial melting equilibria for metapelites *in* Journal of Metamorphic Geology, 25, 511-527.

FIGURES

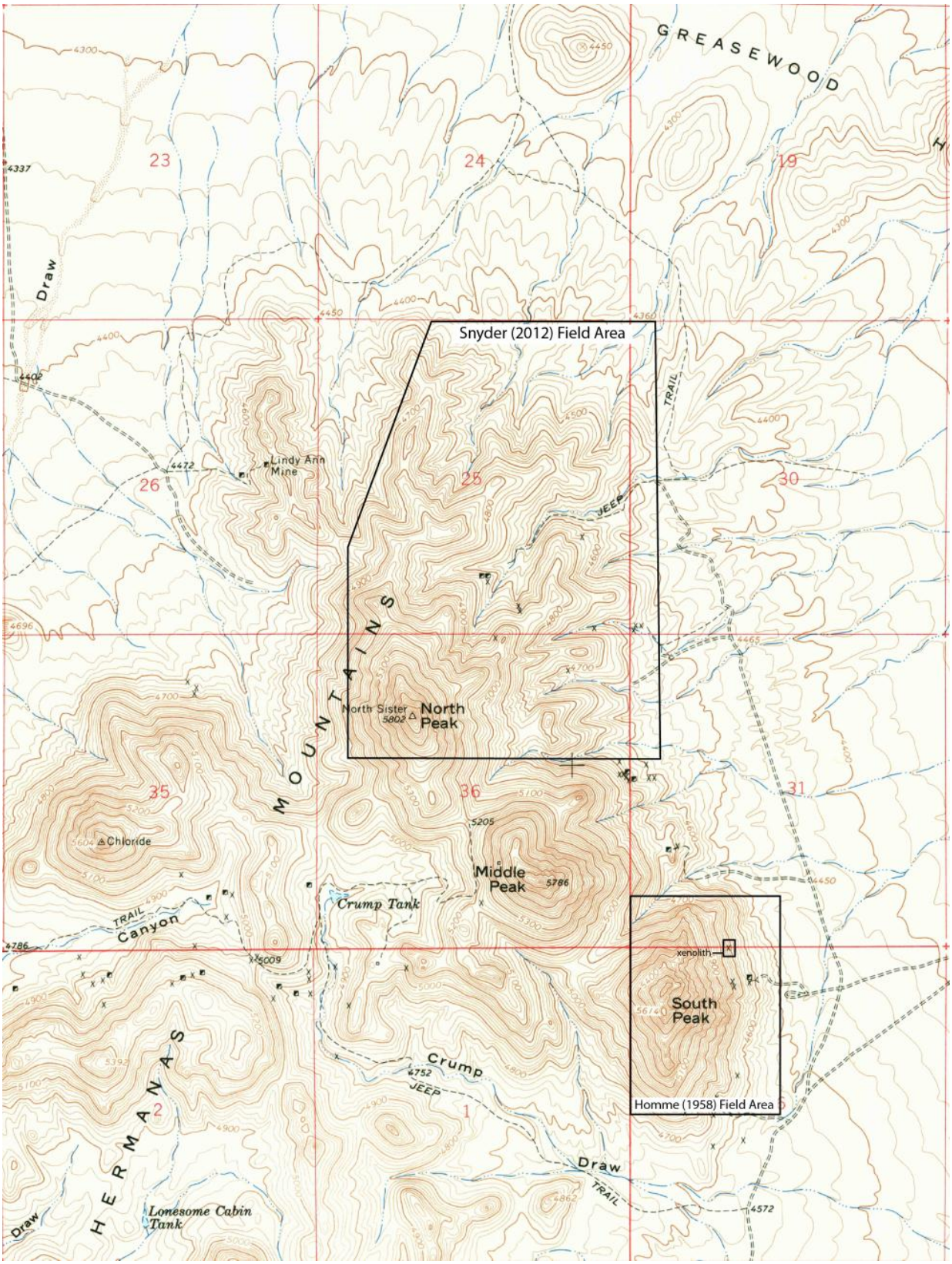

Figure 1. A portion of the North Peak quadrangle showing Snyder (2012) and Homme (1959) field areas.

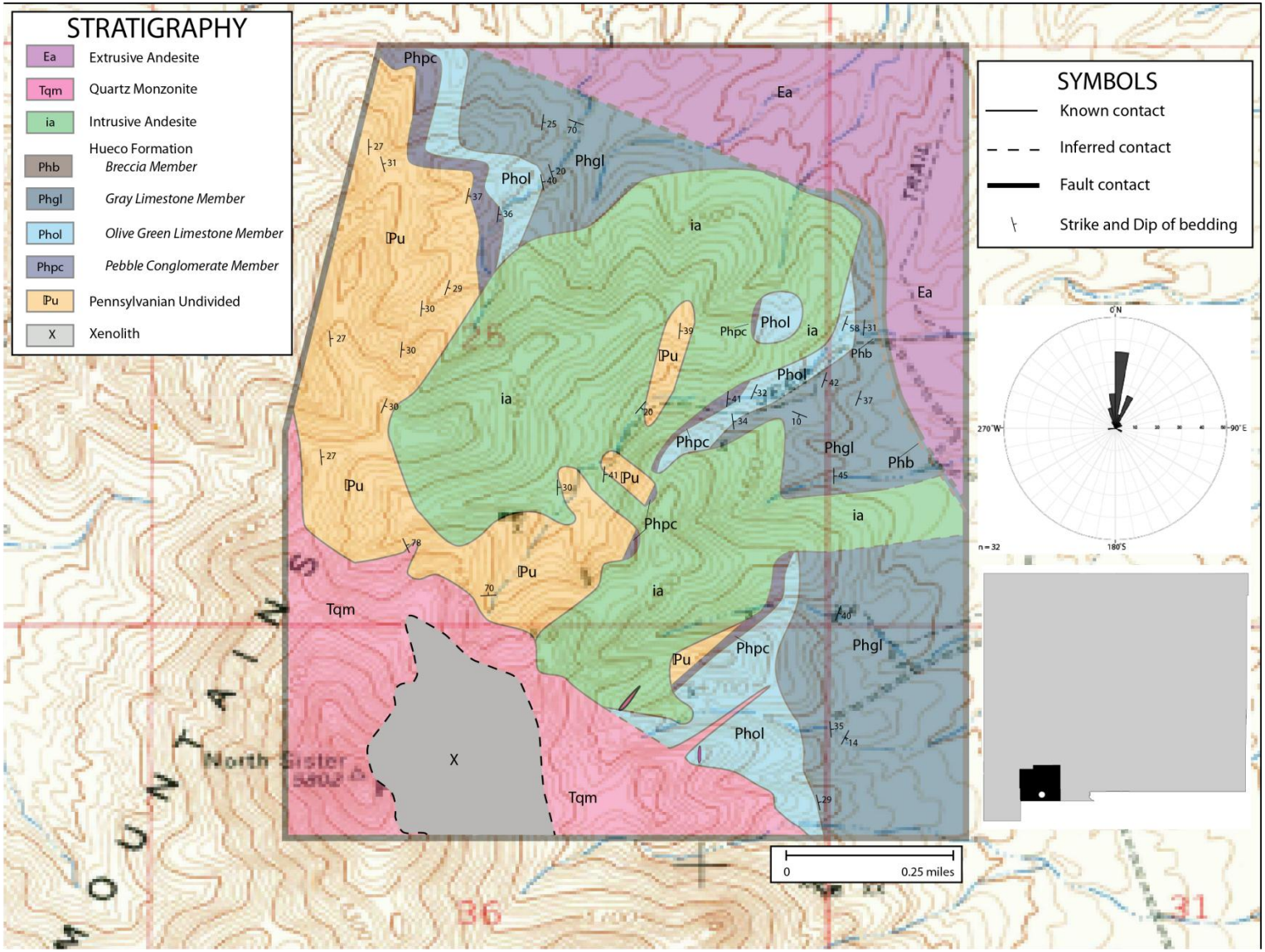

Figure 2 Geologic map of the field area, North Peak, Tres Hermanas Mountains, New Mexico. The bottom inset shows the location of the Tres Hermanas Mountains in Luna County in New Mexico. The rose diagram demonstrates bedding measurements.

Figure 3. Photograph of a large jasper dike sitting atop a quartz monzonite dike (light colored rock below). This photograph is taken approximately due north of North Peak near sample ocation TH12S-071 looking to the southwest.

Figure 4. Deformation and intense mineral growth near vertical andesite intrusions. A) Large radiating wollastonite laths at sample location TH12S-152 B) Deformation in a wollastonite skarn at sample location TH12S-019.

Figure 5. Evidence of the presence of a fluid – brecciated pockets and veins near sample location TH12S-188.

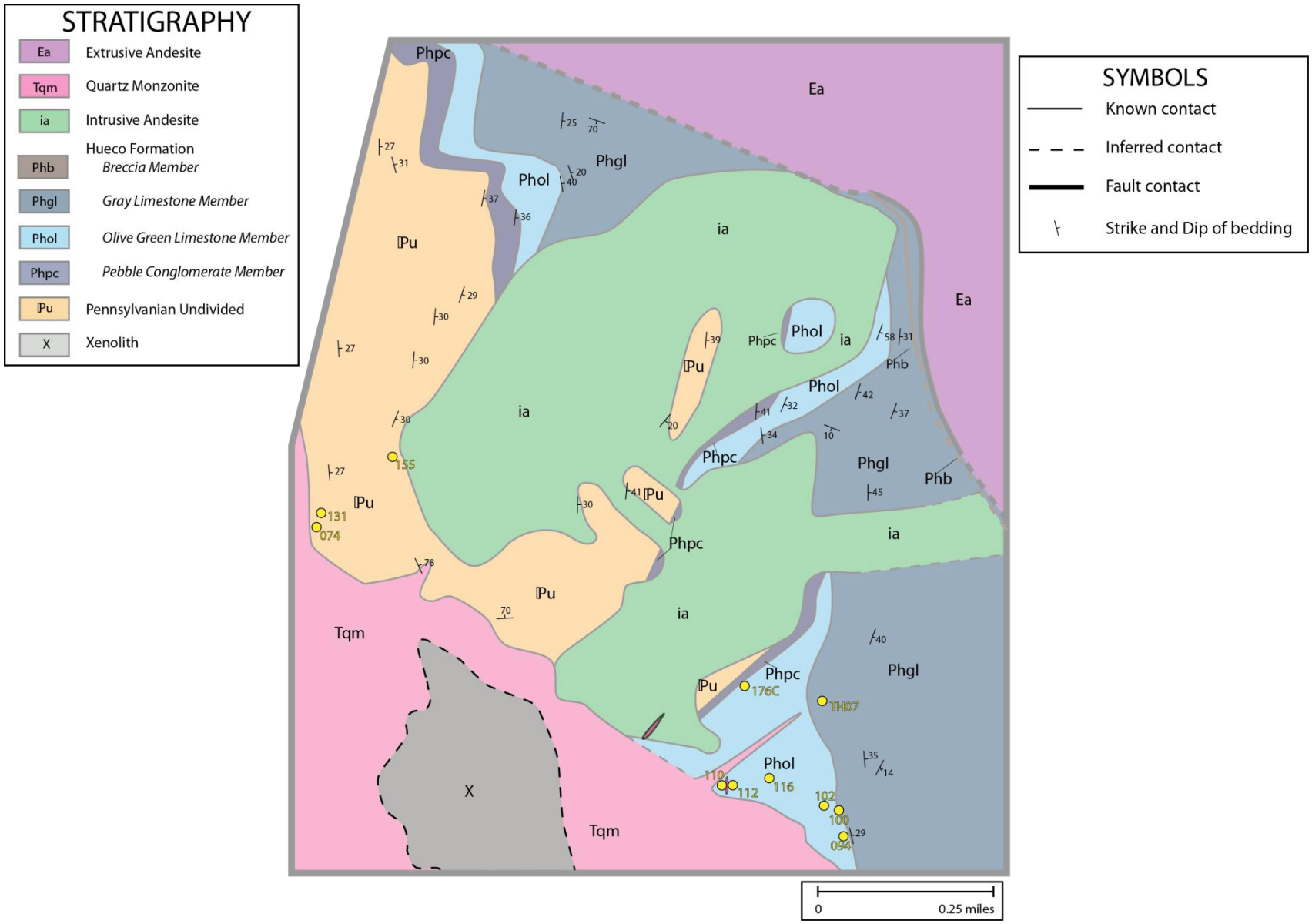

Figure 6. Sample location map.

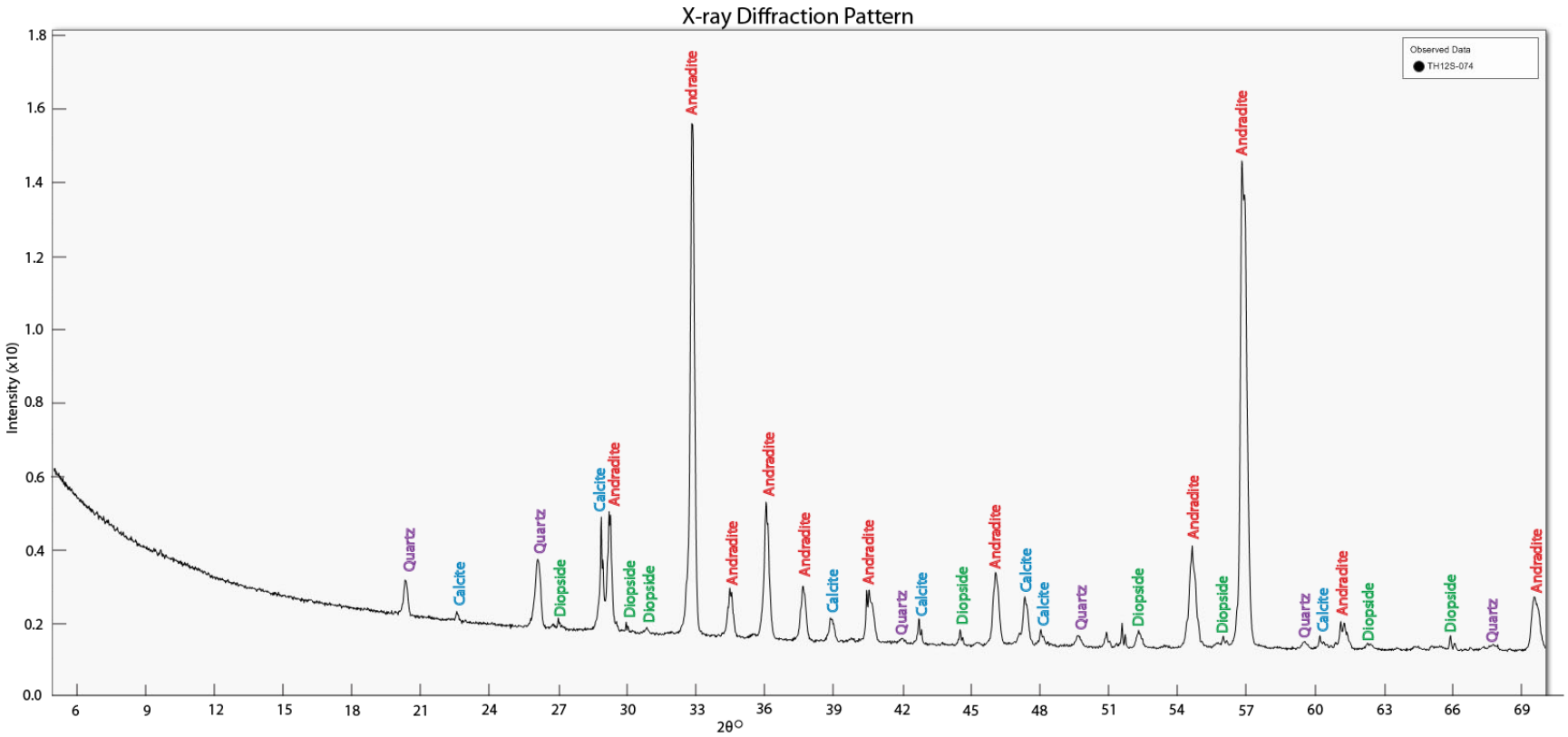

Figure 7. XRD analysis of sample TH12S-074 using Crystal Maker software.

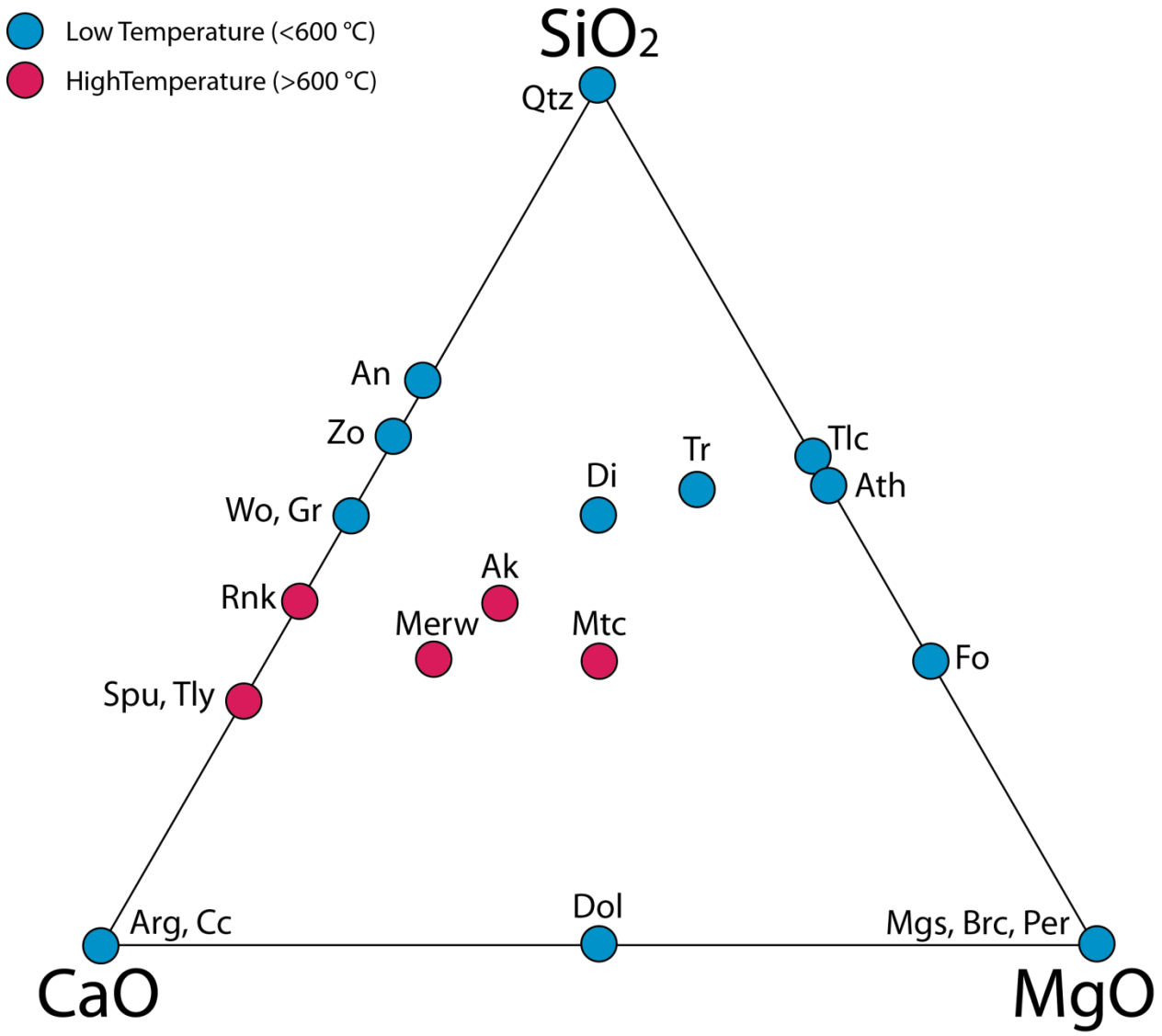

Figure 8. Compositional ternary diagram of progressive carbonate metamorphism. Modified from Heinrich (2007) and Cho and Ernst (1991).

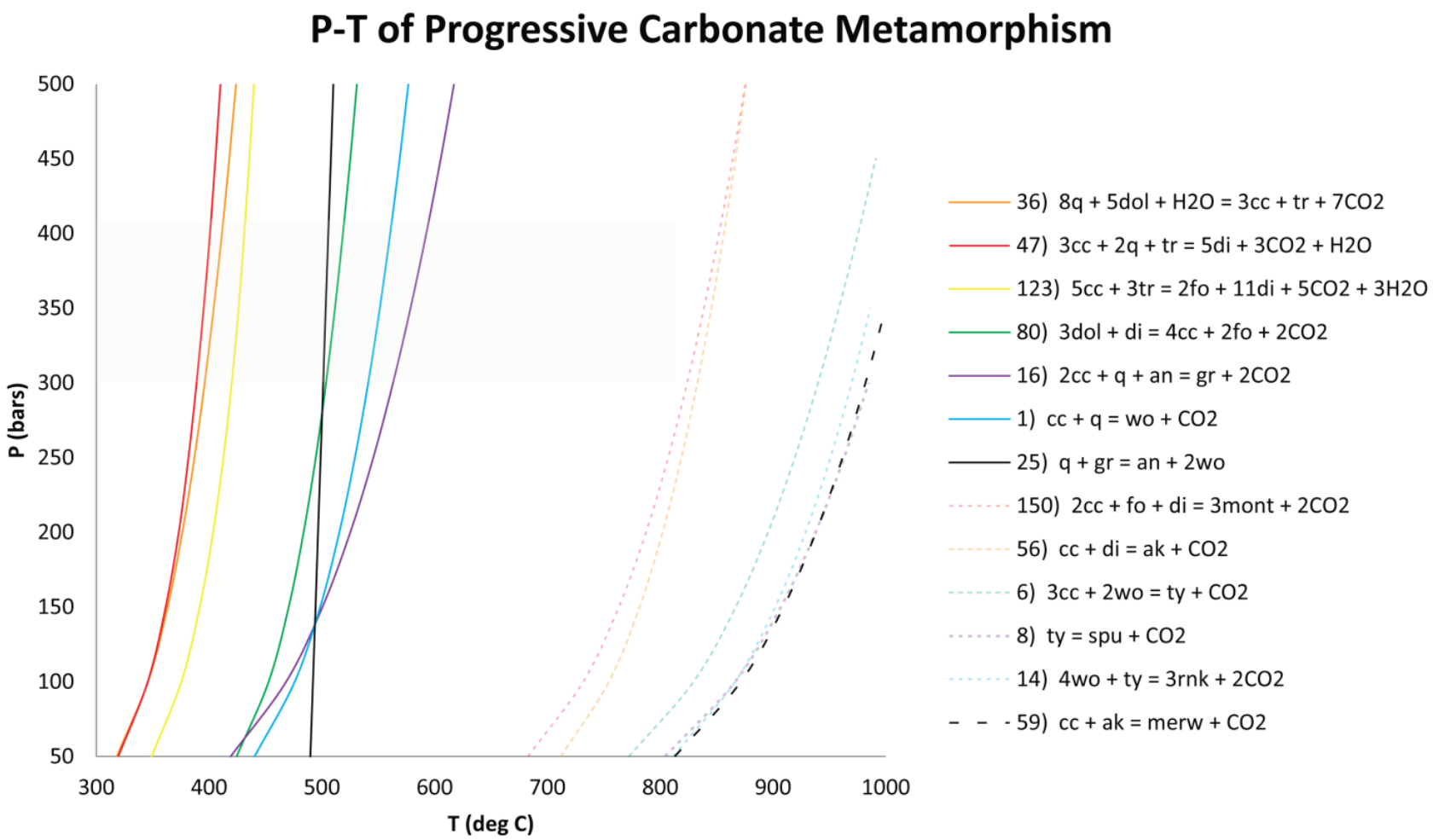

Figure 9. P-T diagram of suspected metamorphic reactions. Shaded region shows range in pressure expected for the Tres Hermanas Mountain contact-metamorphic aureole. Bold colored lines demonstrate the low-temperature assemblages observed in the aureole.

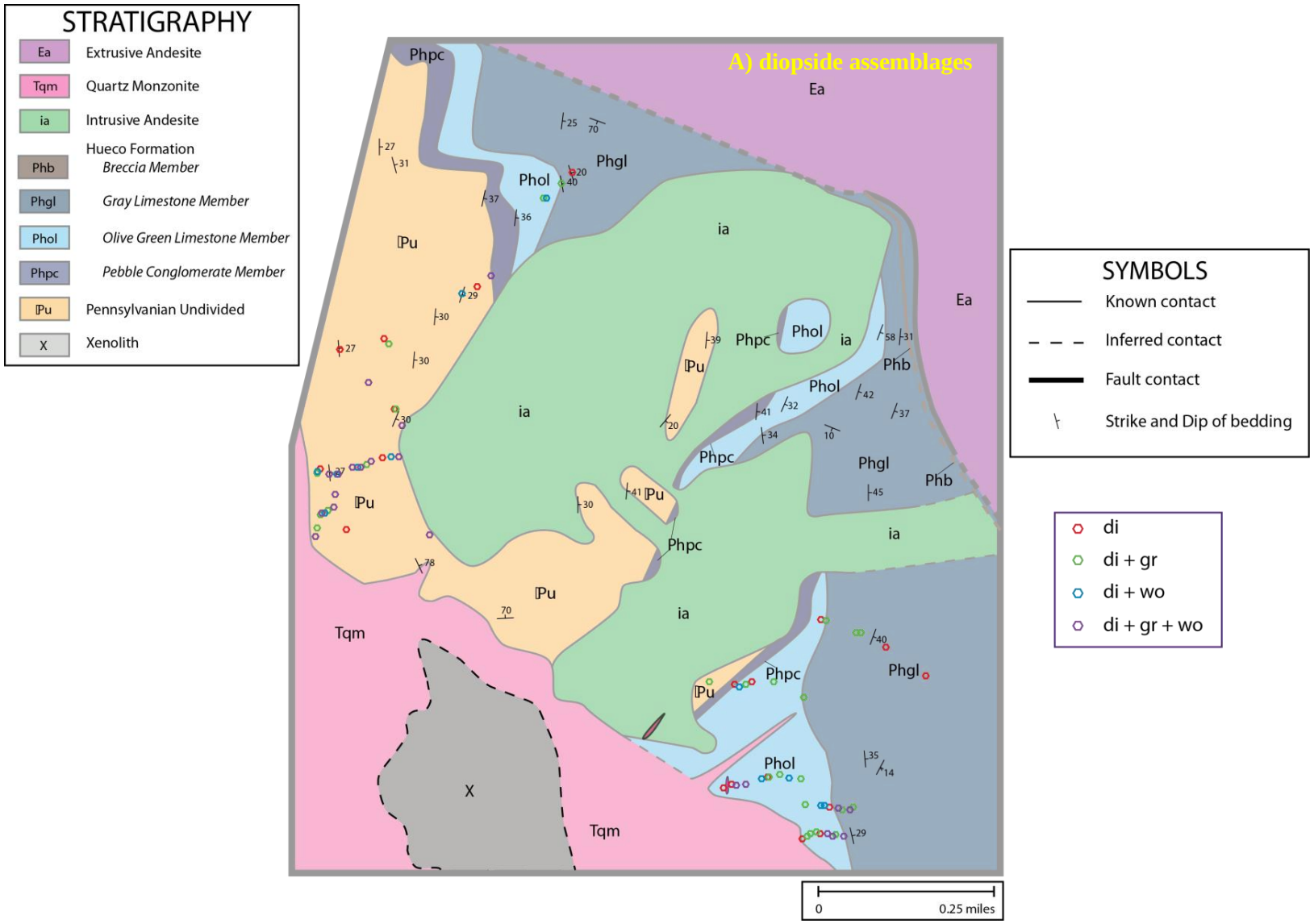

Figure 10. Maps showing the spatial distribution of metamorphic assemblages. A) diopside assemblages, B) garnet assemblages, and C) wollastonite assemblages.

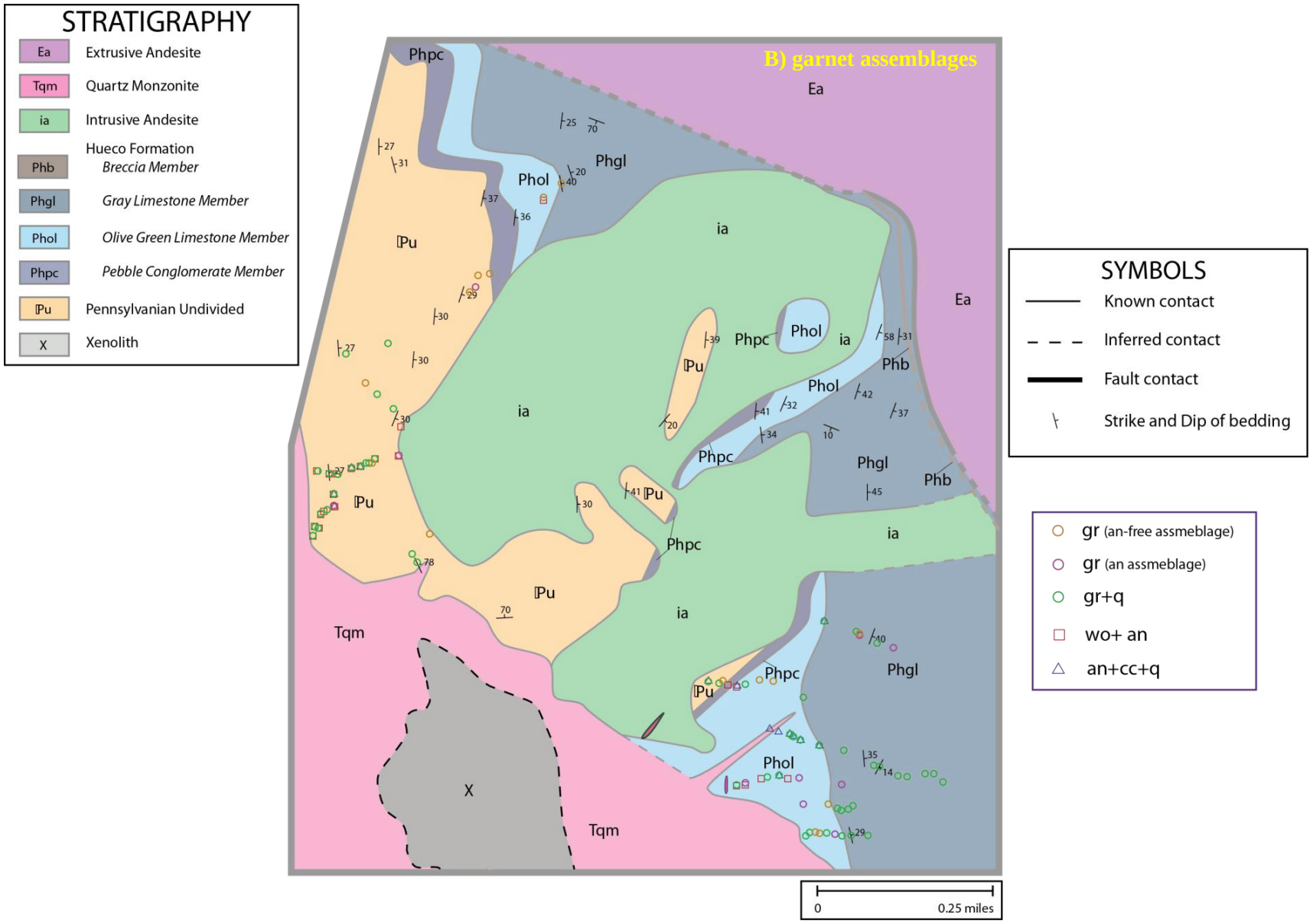
STRATIGRAPHY
Ea
Extrusive Andesite
Tqm
Quartz Monzonite
ia
Intrusive Andesite
Hueco Formation
Phb
Breccia Member
Phgl
Gray Limestone Member
Phol
Olive Green Limestone Member
Phpc
Pebble Conglomerate Member
IPu
Pennsylvanian Undivided
X
Xenolith
B) garnet assemblages
Phpc
Ea
Phgl
Phol
ia
IPu
Phpc
Phol
ia
Ea
Phb
Phol
Phpc
Phgl
Phb
IPu
ia
Phpc
IPu
Tqm
ia
Phpc
Phgl
IPu
Phol
X
Tqm
0
0.25 miles
SYMBOLS
Known contact
Inferred contact
Fault contact
Strike and Dip of bedding
gr (an-free assmeblage)
gr (an assmeblage)
gr+q
wo+ an
an+cc+q

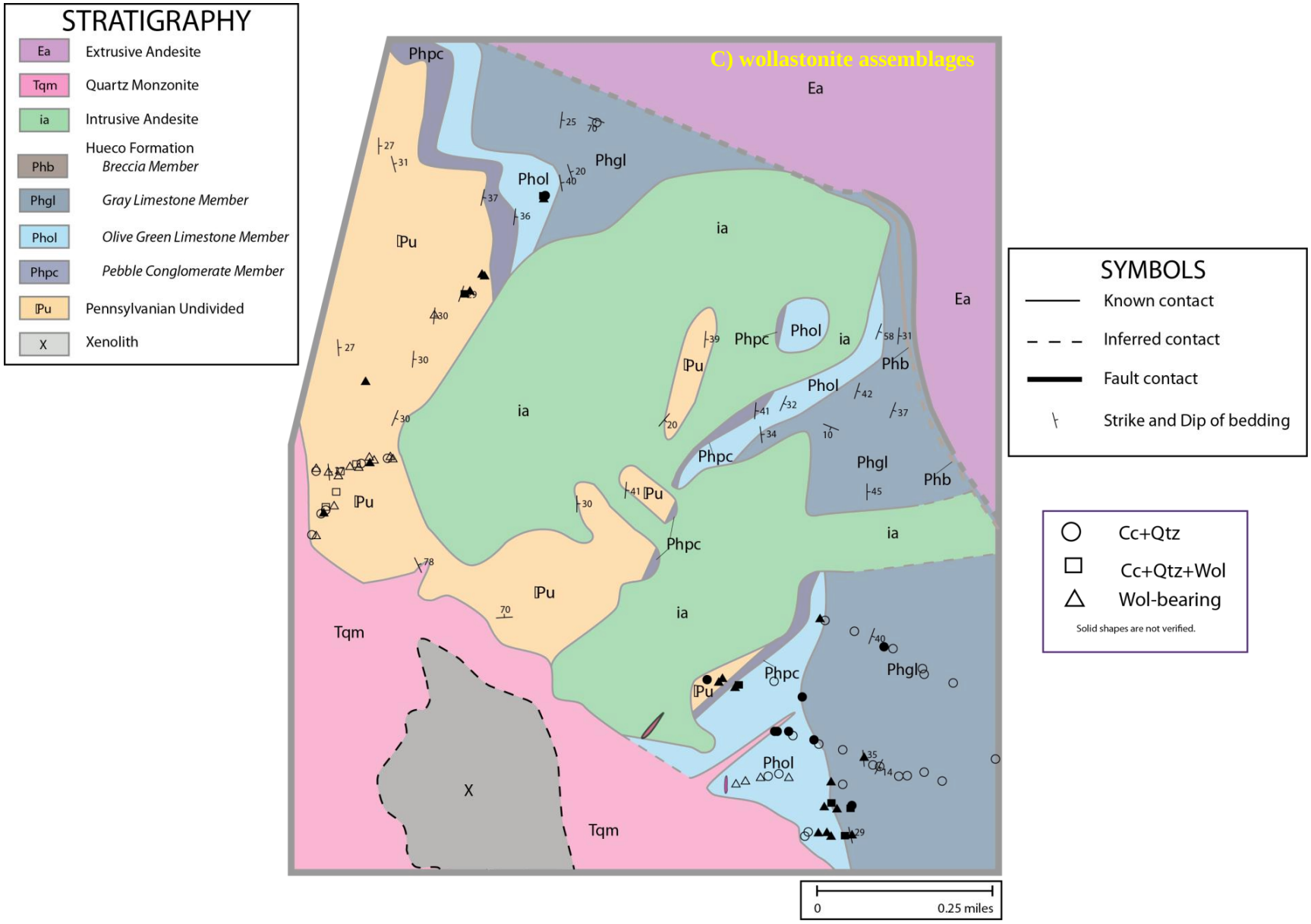
STRATIGRAPHY
Ea Extrusive Andesite
Tqm Quartz Monzonite
ia Intrusive Andesite
Hueco Formation
Phb Breccia Member
Phgl Gray Limestone Member
Phol Olive Green Limestone Member
Phpc Pebble Conglomerate Member
Pu Pennsylvanian Undivided
X Xenolith
C) wollastonite assemblages
Phpc
Ea
Phgl
Phol
ia
Pu
Tqm
X
SYMBOLS
Known contact
Inferred contact
Fault contact
Strike and Dip of bedding
Cc+Qtz
Cc+Qtz+Wol
Wol-bearing
Solid shapes are not verified.
0
0.25 miles

Figure 11. Bleached limestone observed in the Pennsylvanian Undivided Unit and gray Upper Limestone Member of the Hueco Formation observed near sample location TH12S-189, -190, and -217.

Figure 12. Silicified limestone in the gray Upper Limestone Member of the Hueco Formationnear near sample locations TH12S-192 and -214.

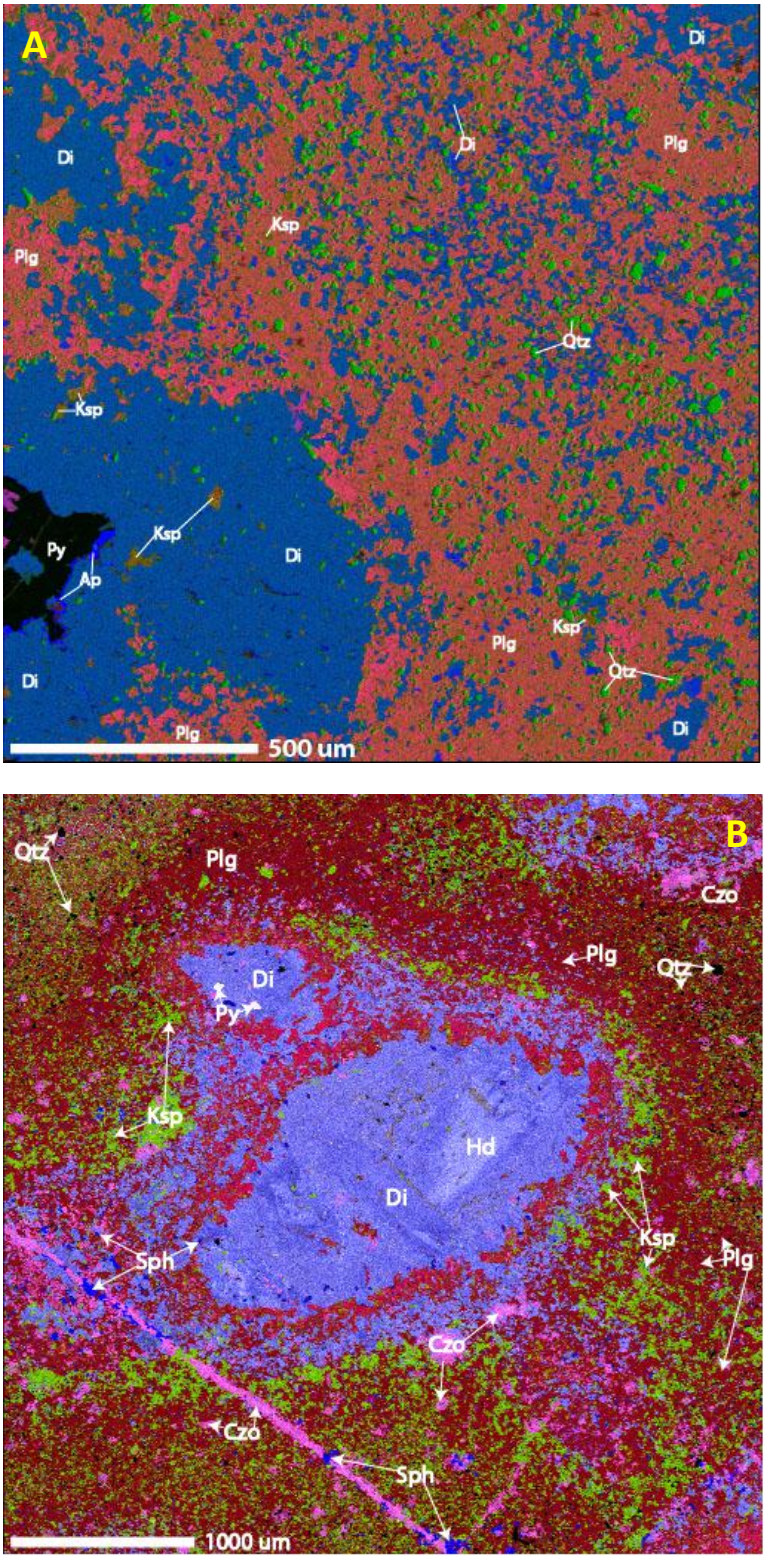

Figure 13. Composite x-ray images of diopside porphyroblasts. A) Sample TH12S-110 showing a diopside porphyroblast with a large pyrite inclusion. B) Corona-like reaction textures in diopside porphyroblasts from sample TH07A-4 and an clinozoisite vein.

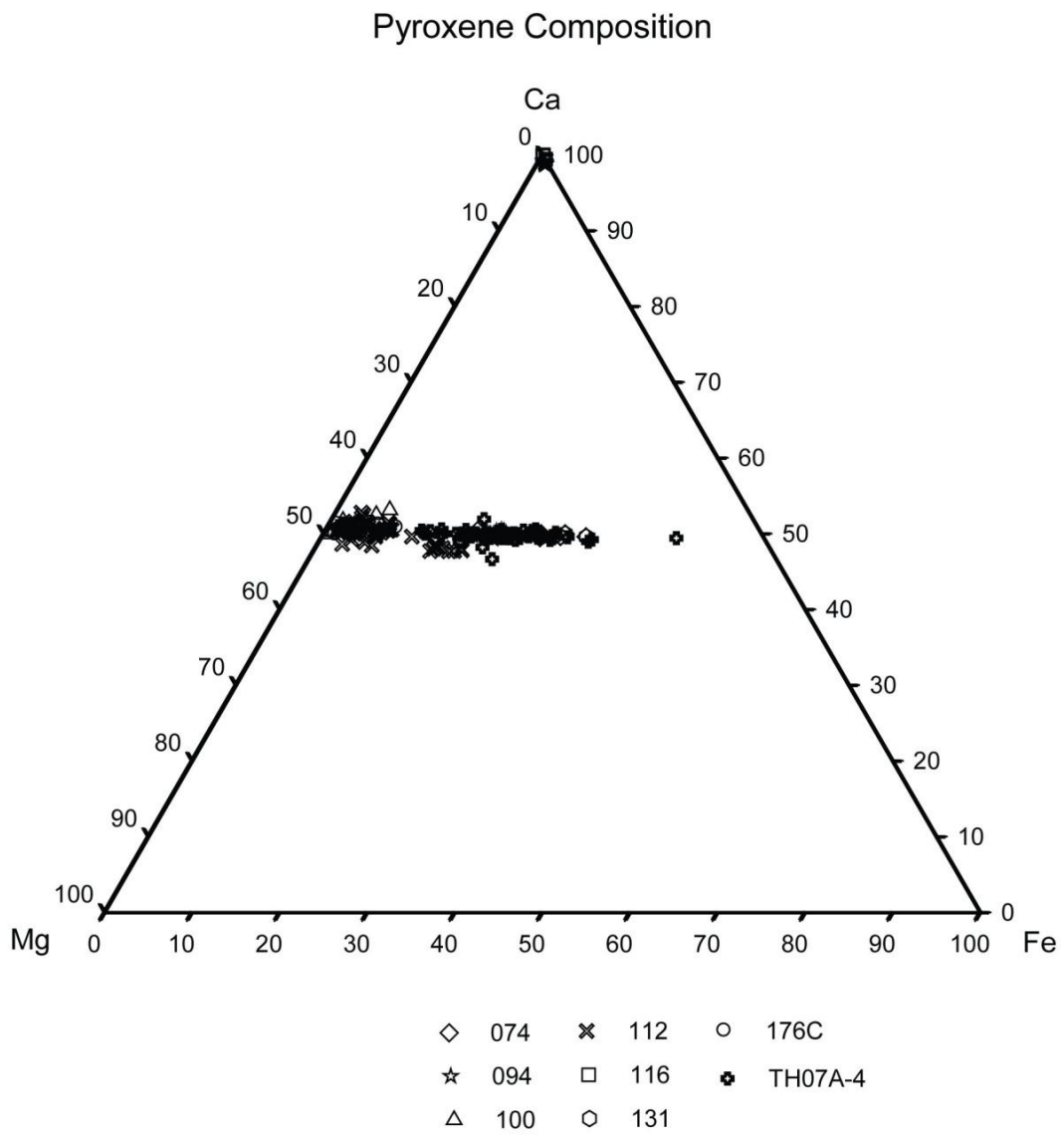

Figure 14. Pyroxene ternary diagram showing diopside-hedenbergite and wollastonite compositions.

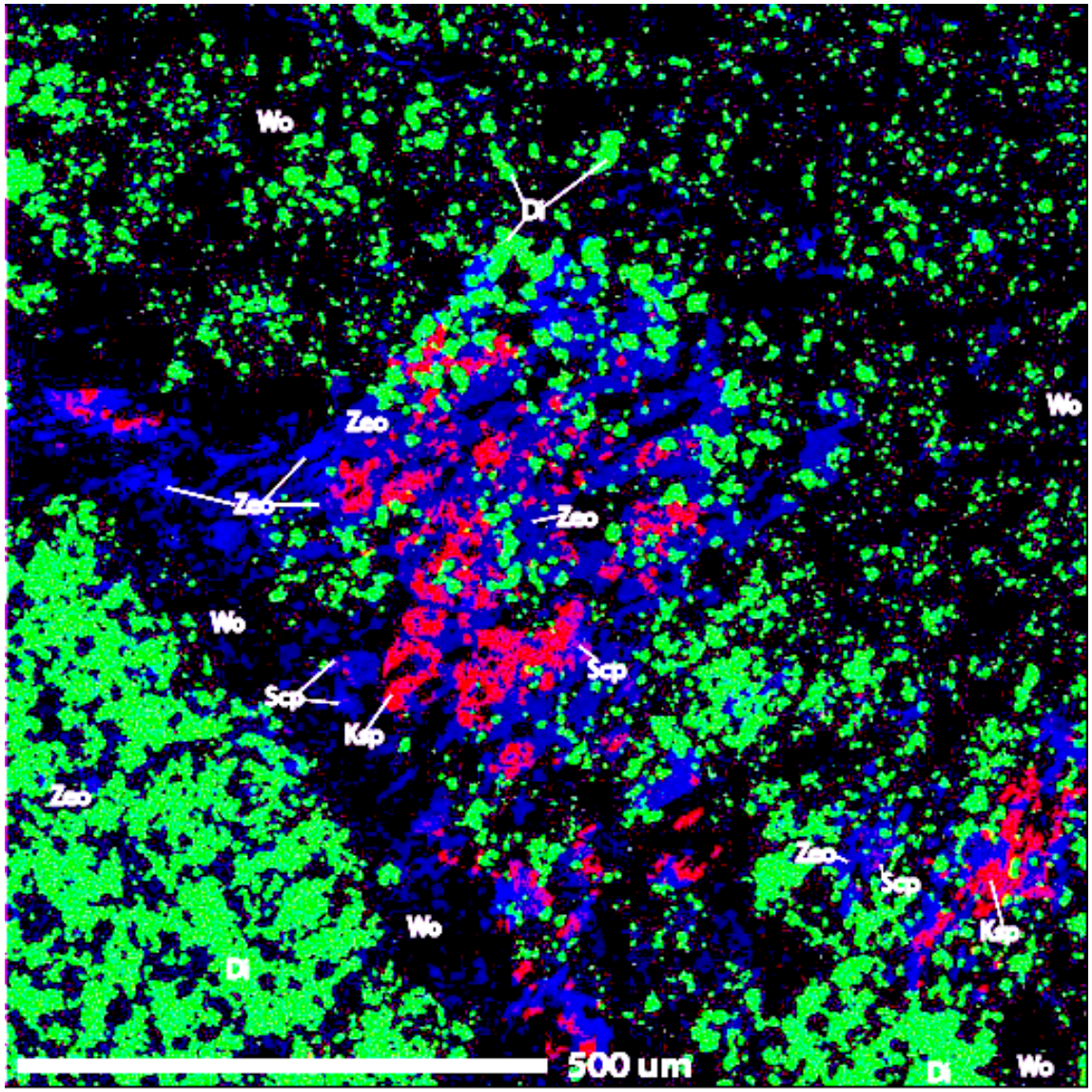

Figure 15. Composite x-ray image demonstrating a reaction pocket near the edge of a large wollastonite grain in sample TH12S-102 The black area is the wollastonite grain, red areas are K-feldspar,green is diopside, and blue is zeolite. Scapolite shows up

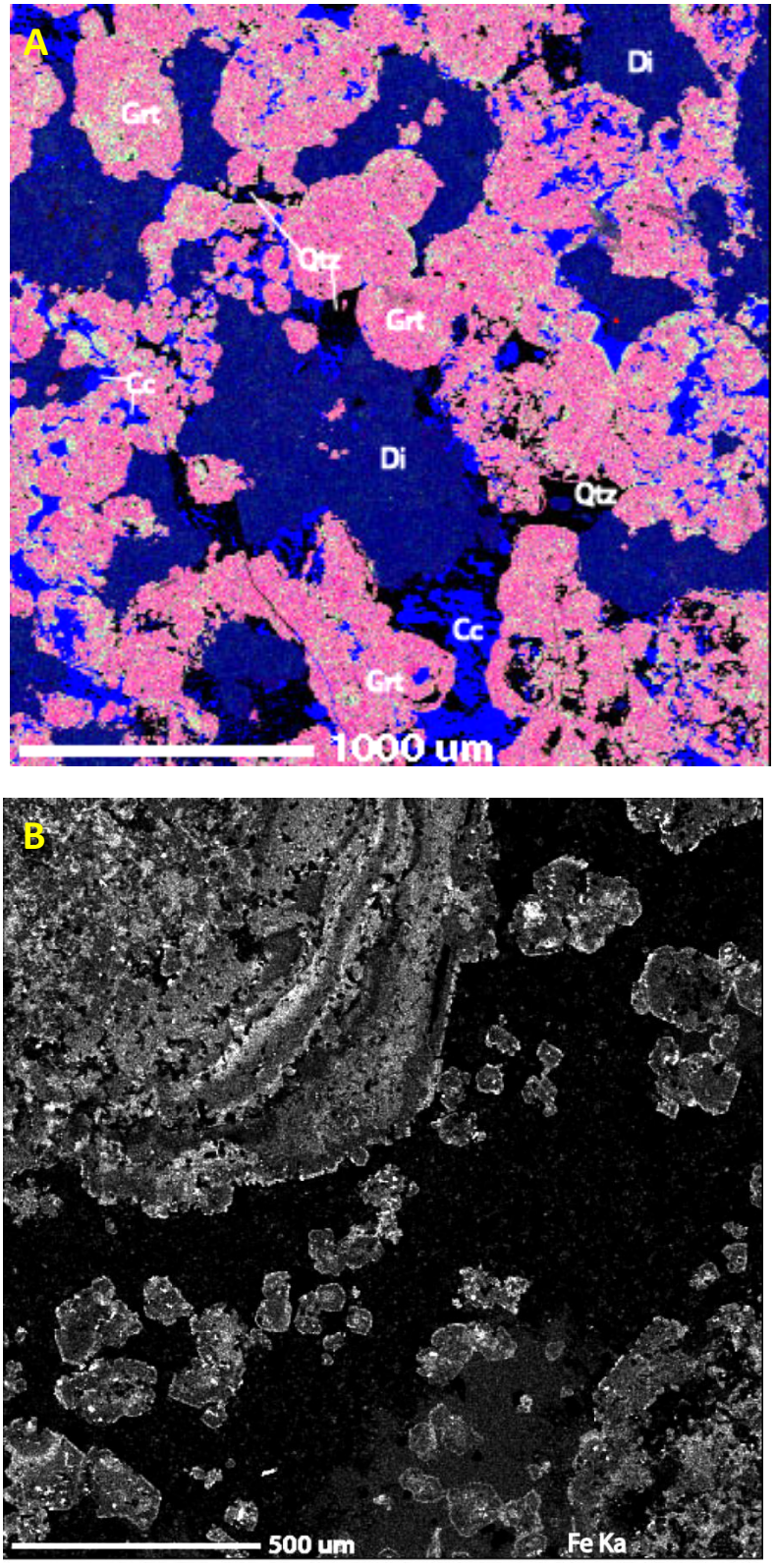

Figure 16. Variations in garnet composition. A) Sample TH12S-074 exhibiting high-aluminum (green) rims on garnet (pink). B) Sample TH12S-094 demonstrating variations in ferric iron content within grains.

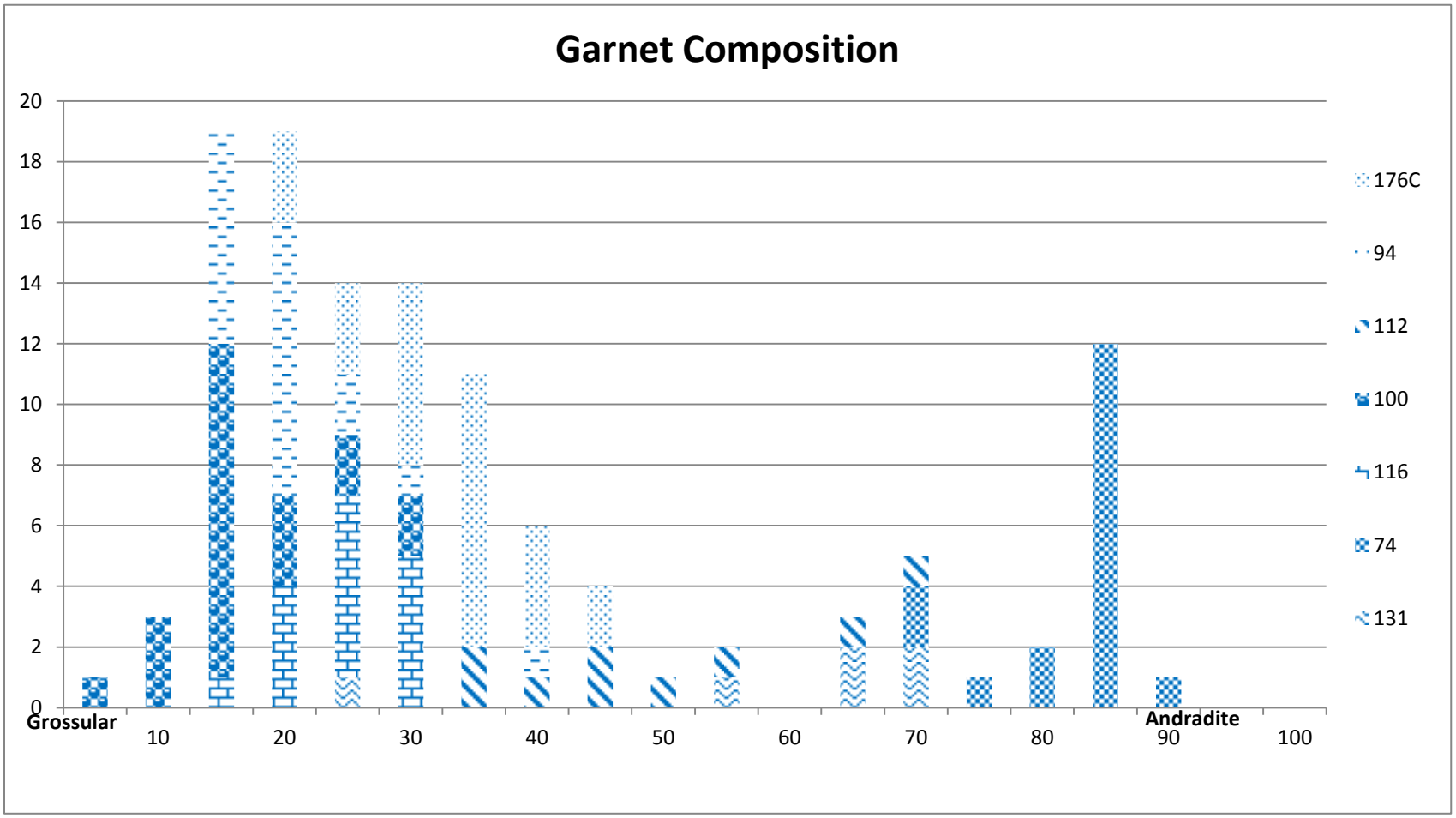

Figure 17. Plot of garnet compositions. Most have a grossular content between 65 - 85 % but a few sampleshave grossular content of 15 - 35 %.

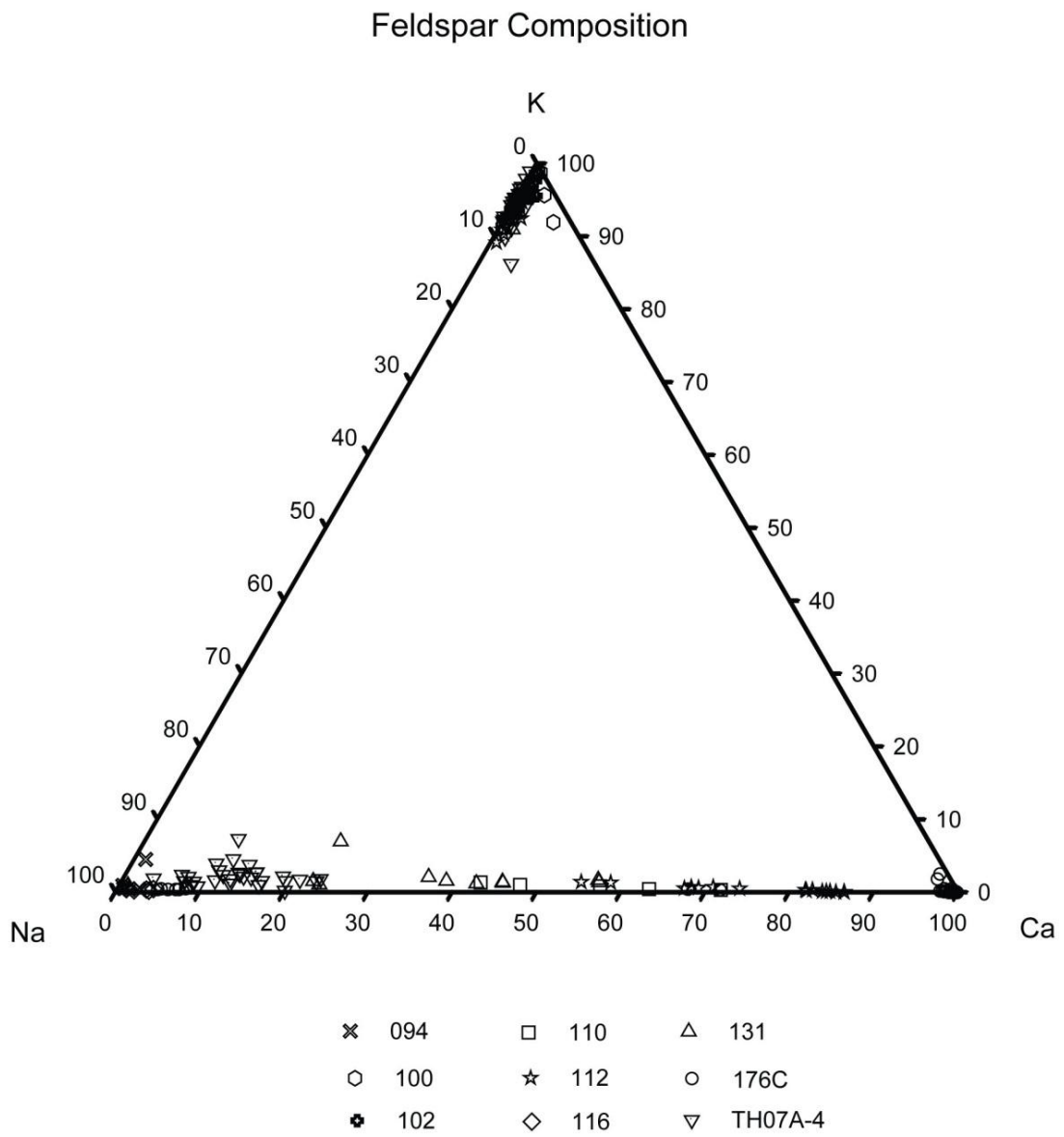

Figure 18. Feldspar ternary diagram showing K-feldspar and a full range in plagioclase composition.

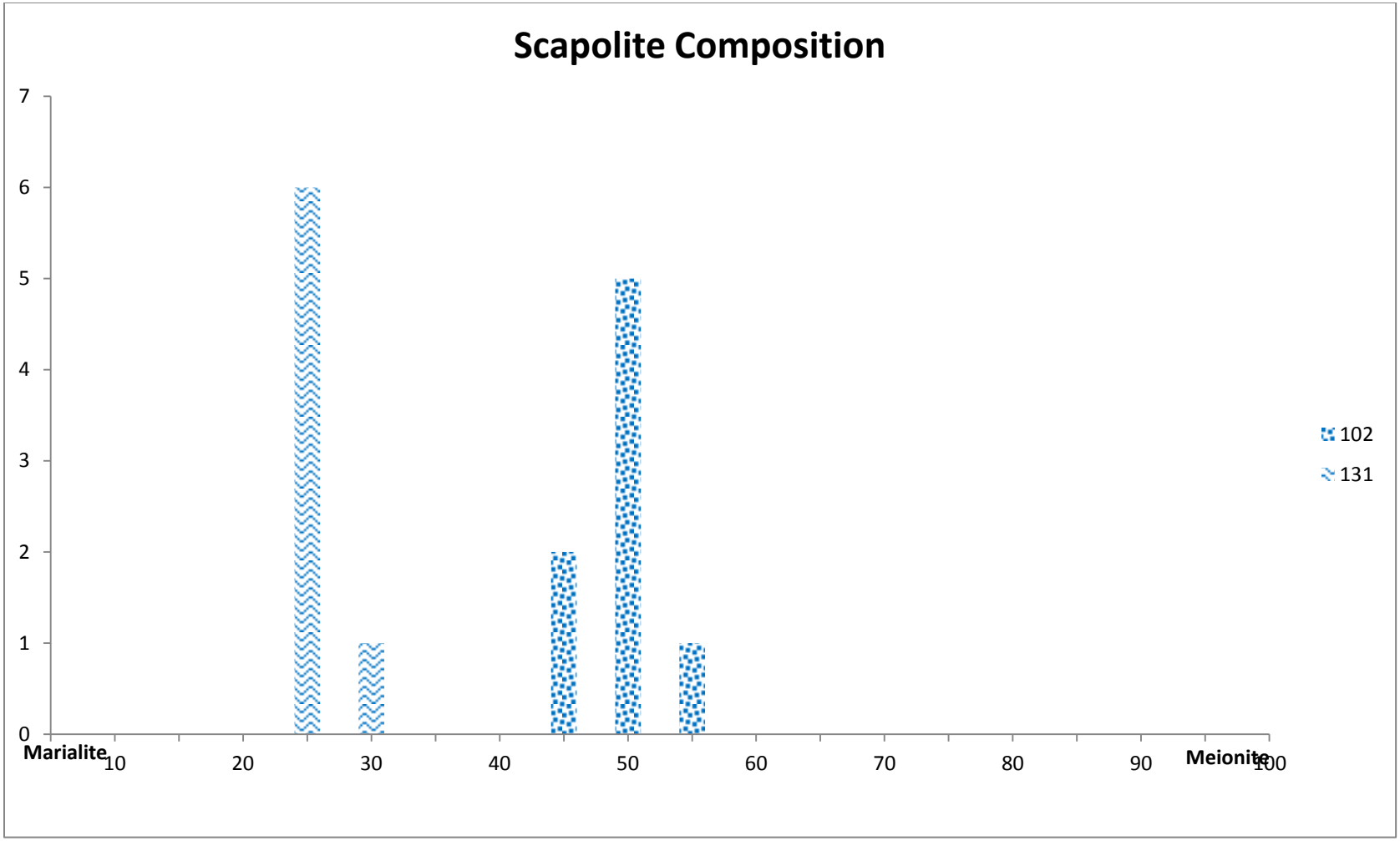

Figure 19. Plot of scapolite compositions. These samples are marialite-like but do not exhibit end-member compositions.

Figure 20. Recrystallized limestone producing a cauliflower-head appearance.

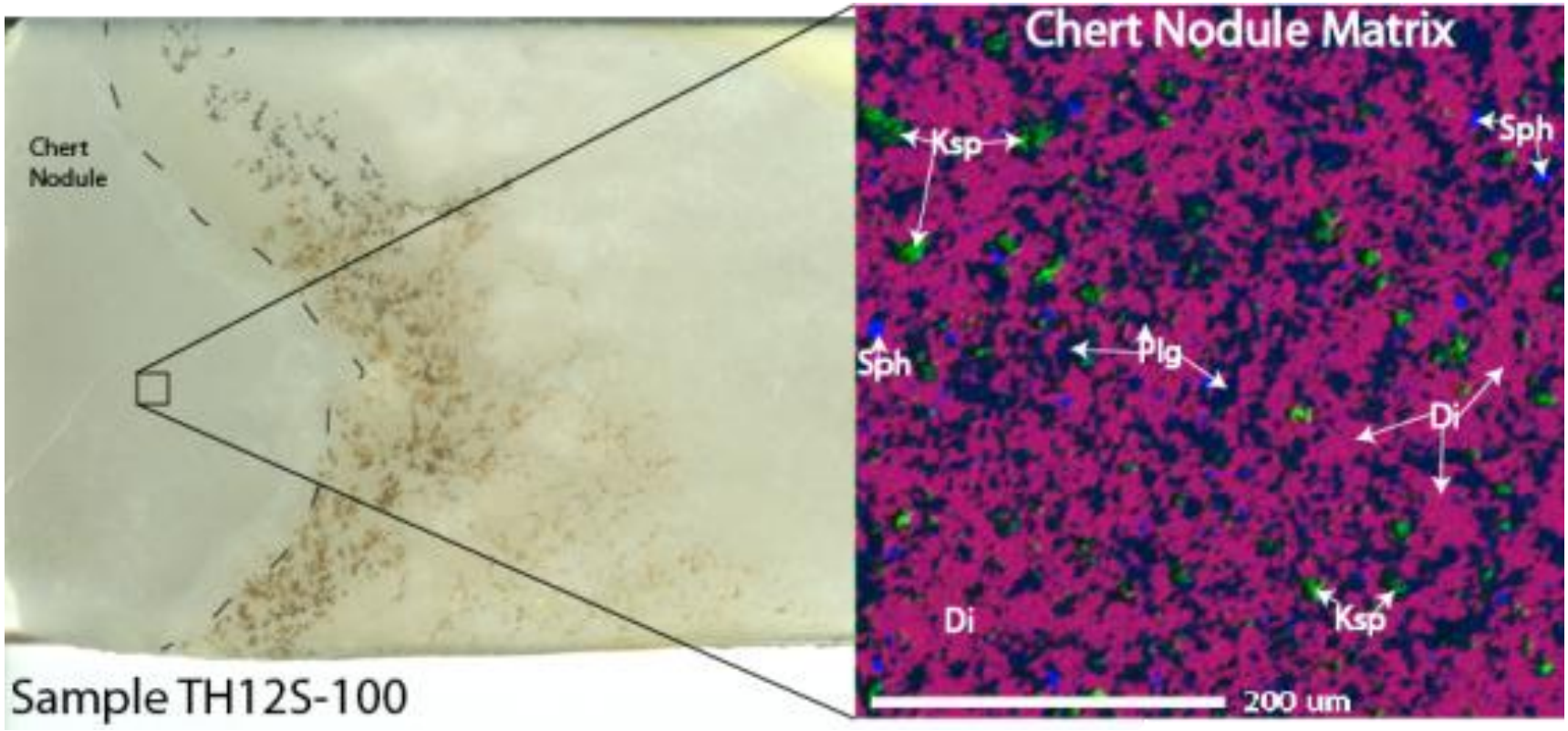

Figure 21. Chert nodule replaced with pyroxene + feldspar.

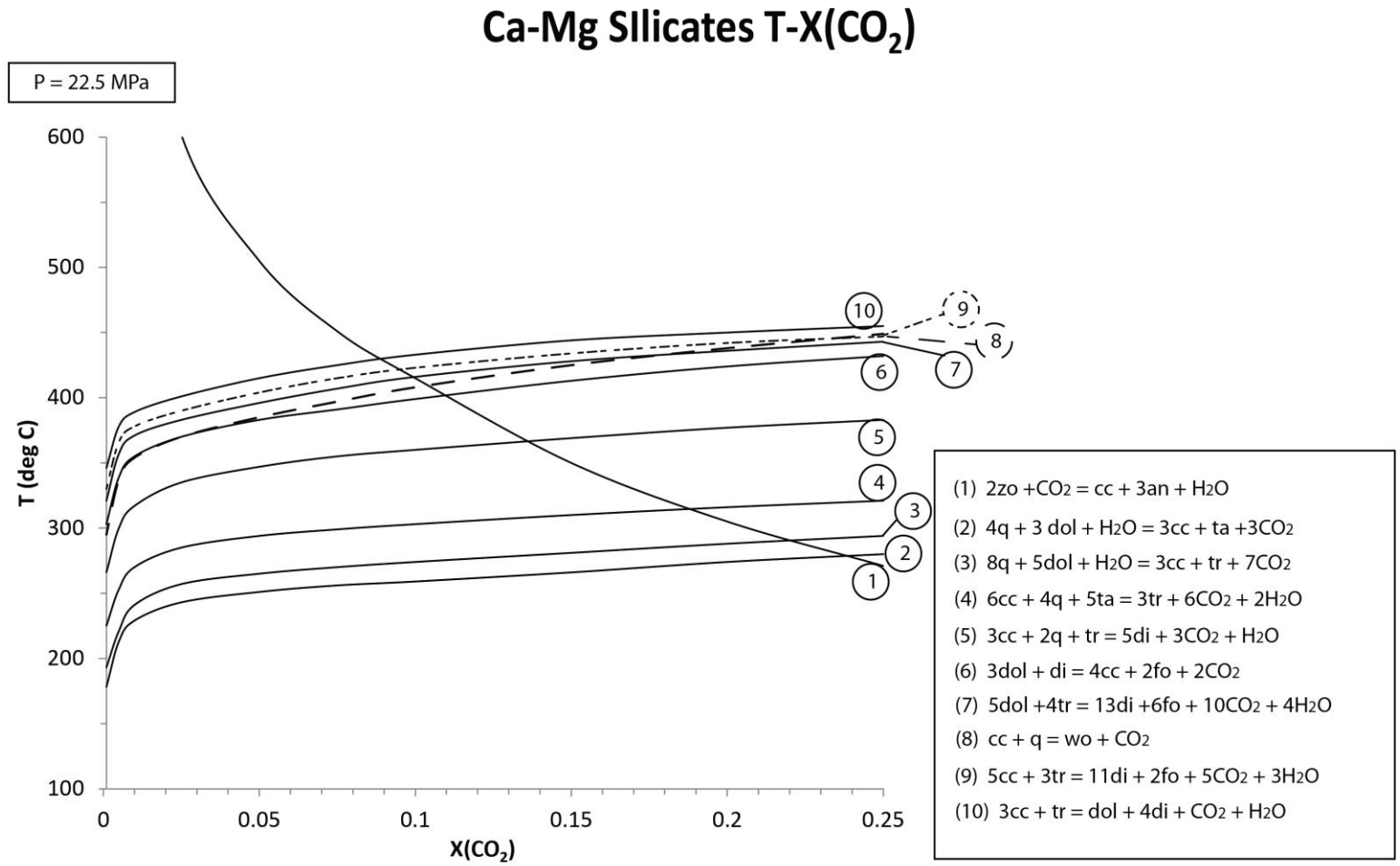

Figure 22. T-X(CO2) diagrams for Ca-Mg silicates.

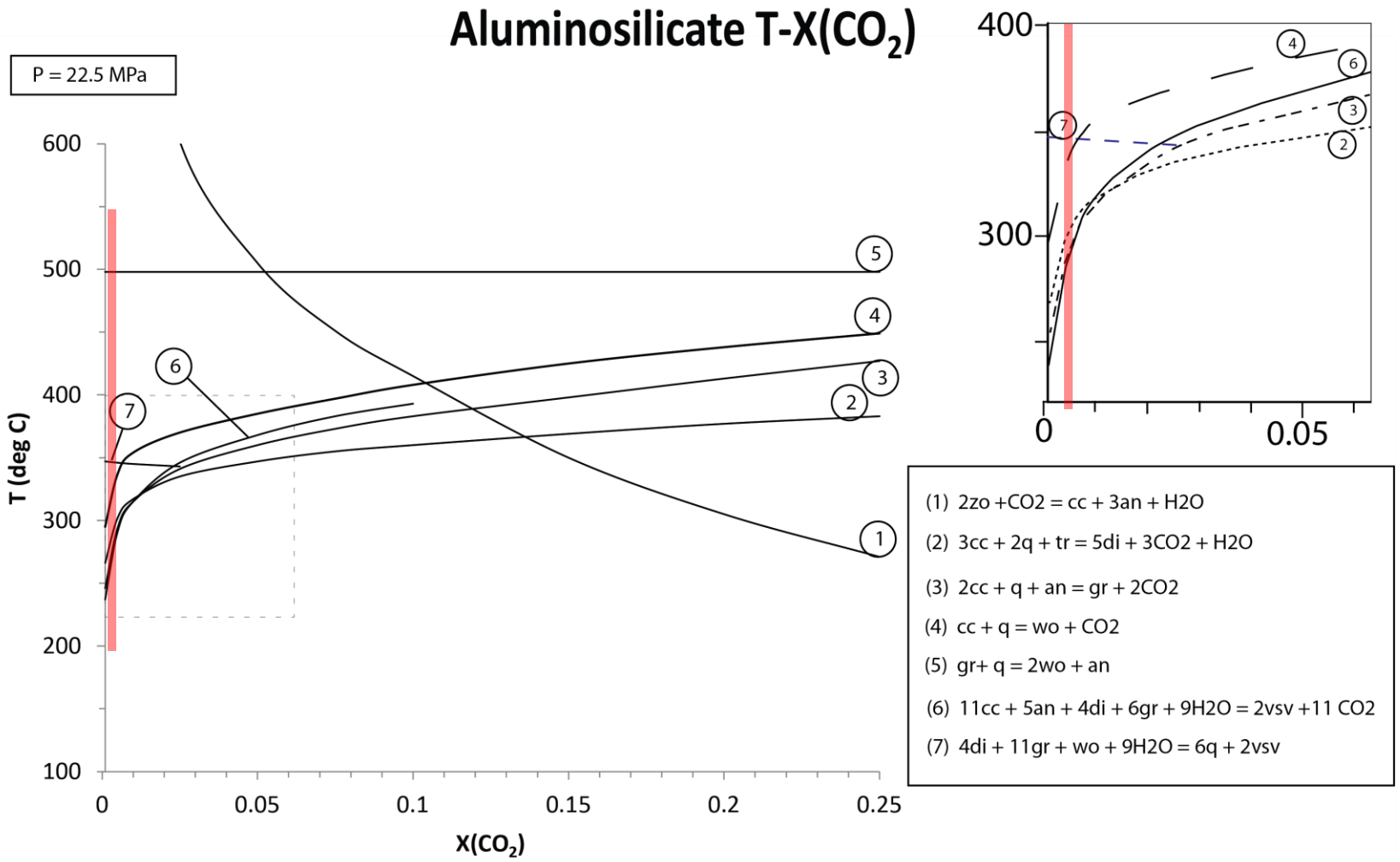

Figure 23. T-X(CO2) diagrams for Aluminous calc-silicates. The inset is a blown up view of the region in the dashed box. The red shaded regions highlight the range in $X(CO_2)$ calculated in this study.

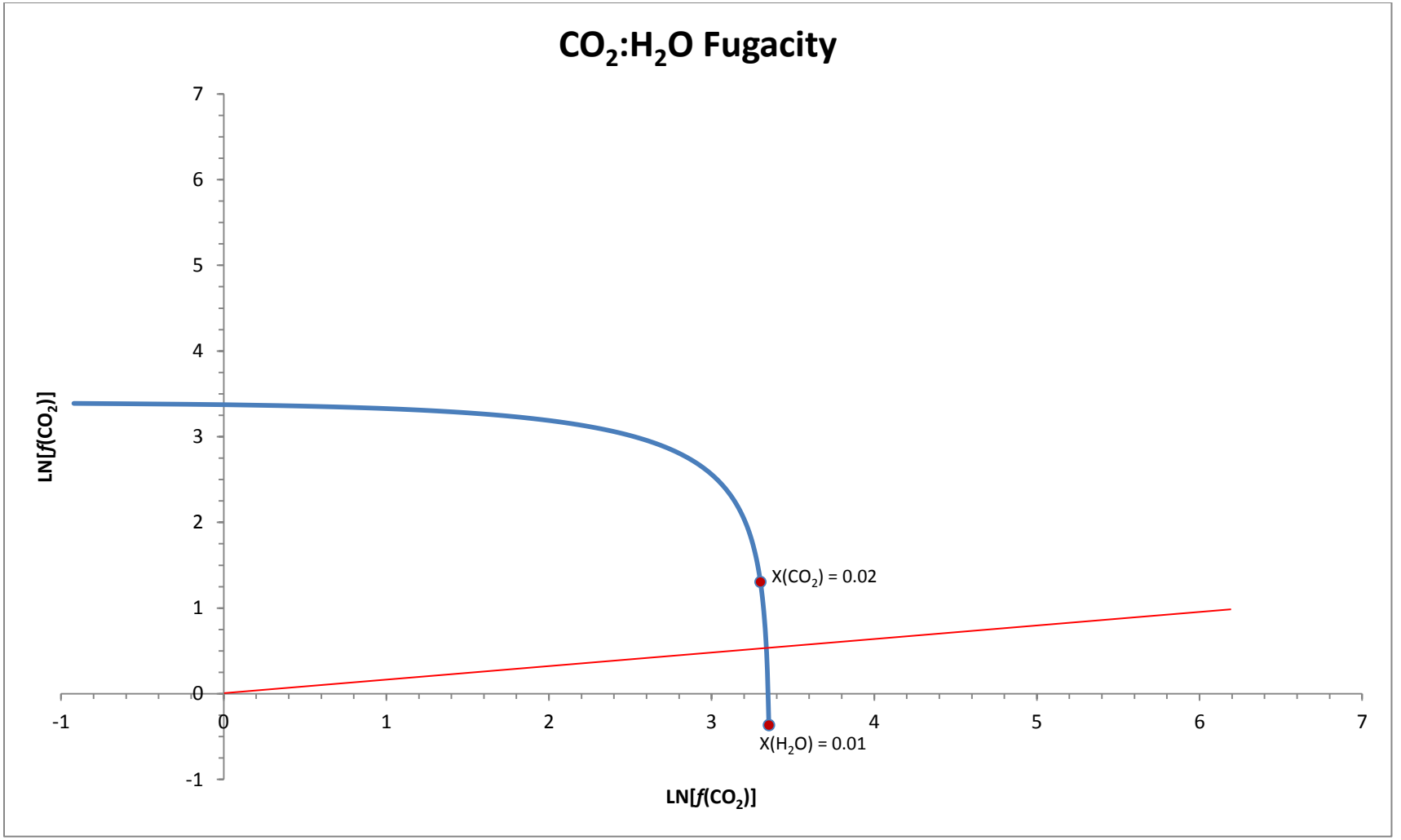

Figure 24. H2O/CO2 fugacity at 30 MPa and 400 °C. The blue line identifies the ideal solution curve and the red line shows the calculated fugacity ratio that crosses the ideal curve between the mole fractions of CO2 between 0.01 and 0.02 .

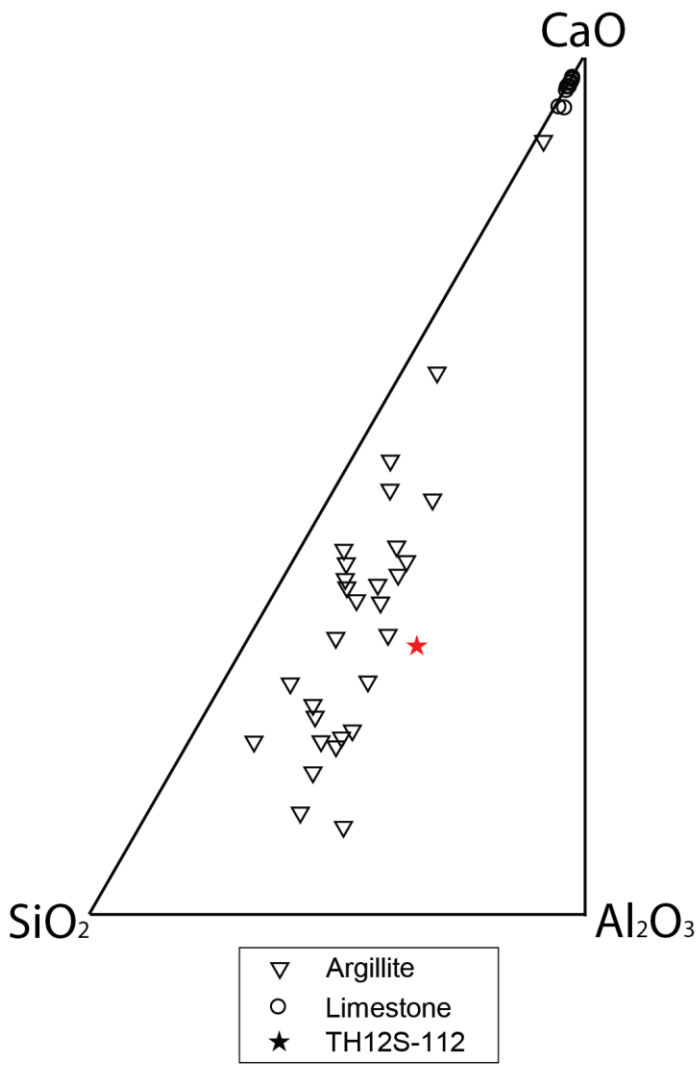

Figure 25. Comparison of Hueco Formation bulk composition to argillite and limestone samples from Notch Peak Aureole, Utah. The open circles are limestones and the open triangles are argillites from the Notch Peak aureole. The red star is the sample from this study. Modified from Labotka et al. (1988).

TABLES

Table 1. Phase assemblages for samples with electron probe microanalysis.

Formation	Sample #	Cc	Qtz	Zeol	Chl	Czo	Plg	Ksp	Scap	Cpx	Gr	Wol	Mica	Sph	Ap	Hem	Py	Sphal
Hueco - upper gray limestone member																		
	TH07A_004		*			*	*			*				*	*		*	*
	TH12S-094		*	*		*		*		*	*			*	*			
	TH12S-100	*	*		*	*		*			*		*	*	*			
Hueco - middle olive-green limestone member																		
	TH12S-102			*		*		*	*	*		*		*				
	TH12S-110					*	*	*		*				*	*		*	
	TH12S-112						*	*		*	*	*		*				
	TH12S-116	*				*	*			*	*			*	*			
	TH12S-176C		*	*	*	*	*	*		*	*			*	*			
Pennsylvanian Undivided																		
	TH12S-074	*	*		*					*	*	*					*	
	TH12S-131					*	*	*	*	*	*							*
	TH12S-155	*	*		*											*		

Table 2. Nomenclature

Name			Abreviations	Formula
akermanite			Ak	$Ca_2MgSi_2O_7$
anthophyllite			Ath	$Mg_7Si_8O_{22}(OH)_2$
aragonite			Arg	$CaCO_3$
biotite			Bt	$K(Mg,Fe)_3AlSi_3O_{10}(OH)_2$
brucite			Brc	MgO
calcite			Cc	$CaCO_3$
carbon dioxide			CO_2	CO_2
clinozoisite			Czo	$Ca_2Al_3Si_3O_{12}(OH)$
diopside			Di	$CaMgSi_2O_6$
dolomite			Dol	$CaMgCO_3$
epidote			Ep	$CaFeAl_2Si_3O_{12}(OH)$
feldspar			Fld	X-$AlSi_3O_8$
forsterite			Fo	$MgSiO_4$
garnet			Grt	X-Al2Si_3O_{12}
	---	andradite	And	$FeAl2Si_3O_{12}$
	---	grossular	Gr	$CaAl2Si_3O_{12}$
K-feldspar			Ksp	$KAlSi_3O_8$
larnite			Lrn	Ca_2SiO_4
magnesite			Mgs	$MgCO_3$
merwinite			Merw	$Ca_3MgSi_2O_8$
monticellite			Mtc	$CaMgSiO_4$
muscovite			Ms	$KAl_3Si_3O_{10}(OH)_2$
periclase			Per	MgO
phlogopite			Phl	$KMg_3Al(OH)_2Si_3O_{10}$
plagioclase			Plg	$(Ca,Na)Al_2Si_2O_8$
	---	albite	Ab	$NaAlSi_2O_8$
	---	anorthite	An	$CaAl_2Si_3O_8$
pyrite			Py	FeS
quartz			Qtz, q	SiO_2
rankinite			Rnk	$Ca_3Si_2O_7$
scapolite			Scp	$Na_2Ca_2Al_5Si_7O_{24}Cl$
	---	marialite	Ma	$Na_4Al_3Si_9O_{24}Cl$
	---	meionite	Me	$Ca_4Al_6Si_6O_{24}CO_3$
sphalerite			Sph	ZnS
sphene			Spn	$CaTiSiO_5$
spurrite			Spr	$2Ca_2SiO_4{\cdot}CaCO_3$
talc			Tlc, Ta	$Mg_3Si_4O_{10}$

tilleyite	Tly	$Ca_3Si_2O_7 \cdot 2CaCO_3$
tremolite	Tr	$Ca_2Mg_5Si_8O_{22}(OH)_2$
vesuvianite	Vsv	$Ca_{19}Mg_2Al_{11}Si_{18}O_{69}(OH)_9$
water	H_2O	H_2O
wollastonite	Wo	$CaSiO_3$
zoisite	Zo	$Ca_2Al_3Si_3O_{12}(OH)$

Table 3. List of metamorphic reactions from low-grade to high-grade with low-temperature assemblages on the left side of each reaction.

	Reaction		
Rxn #	Low T assemblage		High T assemblage
1	4q + 3dol + H_2O	↔	3cc + ta + 3CO_2
2	8q + 5dol + H_2O	↔	3cc + tr + 7CO_2
3	6cc + 4q + 5ta	↔	3tr + 6CO_2 + 2H_2O
4	3cc + 2q + tr	↔	5di + 3CO_2 + H_2O
5	cc + q + an	↔	gr + 2CO_2
6	3dol + di	↔	4cc + 2fo + 2CO_2
7	cc + q	↔	wo + CO_2
8	5dol + 4tr	↔	13di + 6fo + 10CO_2 + 4H_2O
9	5cc + 3tr	↔	11di + 2fo + 5CO_2 + 3H_2O
10	3cc + tr	↔	dol + 4di + CO_2 + H_2O
11	q + gr	↔	2wo + an
12	11cc + 5an + 4di + 6gr + 9H_2O	↔	2vsv + 11CO_2
13	4di + 11gr + wo + 9H_2O	↔	6q + 2vsv
14	2zo + CO_2	↔	cc + 3an + H_2O
15	3an + cc	↔	me

Table 4. Representative Weight % Analyses of Pyroxene

Sample #	74	74	131	116	100
SiO2	54.10	50.91	51.41	54.01	53.83
TiO2	n.d.	n.d.	0.04	0.05	0.10
Al2O3	1.04	0.08	0.43	0.53	0.91
Cr2O3	n.d.	n.d.	0.04	n.d.	0.03
MgO	17.38	n.d.	8.67	16.32	15.89
CaO	25.80	48.02	23.67	25.34	25.39
MnO	0.41	0.10	0.30	0.30	0.15
FeO*	1.41	0.39	14.96	3.44	3.97
Na2O	n.d.	0.03	0.22	0.08	0.08
K2O	n.d.	0.07	n.d.	n.d.	n.d.
Total	100.17	99.61	99.74	100.10	100.37

Cations based on 6 oxygens

Sample #	74	74	131	116	100
Si	1.99	1.99	1.99	1.98	1.97
Ti			0.00	0.00	0.00
Al	0.00	0.00	0.02	0.02	0.04
Cr			0.00		0.00
Mg	0.00		0.50	0.89	0.87
Ca	2.01	2.01	0.98	1.00	1.00
Mn	0.00	0.00	0.01	0.01	0.01
Fe*	0.00	0.01	0.48	0.11	0.12
Na		0.00	0.02	0.01	0.01
K		0.00			
Total	4.01	4.02	4.01	4.01	4.01

* Indicates Total iron as Fe+2

Analyses 1 and 2 are from sample 074; analysis 3 is from sample131; analysis 4 is from sample 116; and analysis 5 is from sample 100.

Table 5. Representative Weight % Analyses of Garnet

Sample #	74	74	94	94	116	100	112
SiO2	36.31	35.69	38.16	36.80	38.77	39.17	36.64
TiO2	0.35	0.20	1.10	2.28	0.21	0.33	1.78
Al2O3	6.89	3.75	17.96	12.10	19.09	21.54	10.08
Cr2O3	n.d.	0.03	0.03	0.06	n.d.	n.d.	n.d.
Fe2O3	20.93	26.02	5.60	12.26	5.77	1.80	15.91
Y2O3	n.d.	n.d.	n.d.	n.d.	n.d.	n.d.	n.d.
MgO	0.16	0.18	0.30	0.33	0.20	0.10	0.07
CaO	34.14	33.59	36.31	35.27	35.66	36.57	34.52
MnO	0.28	0.22	0.11	0.13	0.48	0.26	0.19
Na2O	n.d.	n.d.	n.d.	n.d.	n.d.	n.d.	n.d.
Total	99.08	99.68	99.57	99.23	100.21	99.77	99.21

Cations based on 12 oxygens

Sample #	74	74	94	94	116	100	112
Si	2.98	2.97	2.94	2.93	2.96	2.97	2.95
Ti	0.02	0.01	0.06	0.14	0.01	0.02	0.11
Al	0.67	0.37	1.63	1.14	1.72	1.92	0.96
Cr		0.00	0.00	0.00			
Fe	1.29	1.63	0.33	0.73	0.33	0.10	0.96
Y							
Mg	0.02	0.02	0.03	0.04	0.02	0.01	0.01
Ca	3.01	3.00	3.00	3.01	2.92	2.97	2.98
Mn	0.02	0.02	0.01	0.01	0.03	0.02	0.01
Na							
Total	8.01	8.02	8.01	8.00	8.00	8.00	7.98

Analyses 1 and 2 are from sample 074; analyses 3 and 4 are from sample 094; analysis 5 is from sample 116; analysis 6 is from sample 100; and analysis 7 is from sample 112.

Table 6. Representative Weight % Analyses of Feldspar

Sample #	176C	176C	176C	112	112	194	131
SiO2	64.14	64.39	43.06	47.23	54.14	68.82	60.66
Al2O3	18.58	18.93	36.45	33.23	28.43	19.70	24.28
MgO	n.d.	n.d.	n.d.	n.d.	n.d.	n.d.	n.d.
CaO	0.17	0.03	20.34	16.84	11.29	0.16	6.02
FeO*	0.05	0.06	n.d.	0.38	0.35	0.10	0.45
BaO	0.56	1.06	n.d.	n.d.	n.d.	n.d.	
Na2O	0.55	0.62	n.d.	1.91	5.01	11.76	8.04
K2O	16.02	15.48	n.d.	0.07	0.27	0.07	0.18
Total	100.08	100.56	99.92	99.66	99.50	100.61	99.63

Cations based on 8 oxygens

Sample #	176C	176C	176C	112	112	194	131
Si	2.98	2.97	2.00	2.18	2.46	2.99	2.71
Al	1.02	1.03	1.99	1.81	1.52	1.01	1.28
Mg							
Ca	0.01	0.00	1.01	0.83	0.55	0.01	0.29
Fe*	0.00	0.00		0.02	0.01	0.00	0.02
Ba	0.01	0.02					
Na	0.05	0.06		0.17	0.44	0.99	0.70
K	0.95	0.91		0.00	0.02	0.00	0.01
Total	5.01	4.99	5.01	5.01	5.01	5.00	5.00

* Indicates Total iron as Fe+2

Analyses 1,2, and 3 are from sample 176C; analyses 4 and 5 are from sample112; analysis 6 is from sample 194; and analysis 7 is from sample 131.

Table 7. Representative Weight % Analyses of Epidote

Sample #	94	94	100	100	116
SiO2	35.42	35.21	38.87	38.11	37.69
TiO2	2.35	3.07	n.d.	0.08	0.03
Al2O3	13.03	12.70	29.82	26.20	26.88
Cr2O3	n.d.	n.d.	n.d.	n.d.	n.d.
Fe2O3	3.72	3.54	4.49	9.35	8.41
Y2O3	n.d.	n.d.	n.d.	n.d.	n.d.
La2O3	0.51	0.63			
Ce2O3	0.57	1.10			
MgO	4.14	3.98	0.14	0.04	0.05
CaO	34.88	34.43	23.83	23.28	23.92
MnO	0.07	0.08	0.04	n.d.	0.05
Na2O	n.d.	n.d.	n.d.	n.d.	n.d.
Total	94.69	94.74	97.22	97.08	97.03

Cations based on 12 oxygens

Sample #	94	94	100	100	116
Si	2.92	2.91	2.89	2.89	2.86
Ti	0.15	0.19		0.01	0.00
Al	1.26	1.24	2.61	2.34	2.40
Cr					
Fe	0.23	0.22	0.25	0.53	0.48
Y					
La	0.02	0.02			
Ce	0.02	0.03			
Mg	0.51	0.49	0.02	0.00	0.01
Ca	3.08	3.05	1.90	1.89	1.94
Mn	0.01	0.01	0.00		0.00
Na					
Total	8.18	8.15	7.68	7.67	7.70

Analyses 1 and 2 are from sample 094; analyses 3 and 4 are from sample 100; and analysis 5 is from sample 116.

Table 8. Representative Weight % Analyses of Scapolite

Sample #	102	102	131	131	131
SiO2	54.95	54.48	57.45	56.98	57.20
Al2O3	23.67	23.53	21.97	21.92	21.89
MgO	n.d.	n.d.	n.d.	n.d.	n.d.
CaO	7.92	8.05	5.00	5.60	5.42
FeO*	0.14	0.11	0.14	0.18	0.20
Na2O	8.11	8.22	9.55	10.05	9.56
K2O	2.11	2.01	2.03	1.34	1.90
Cl	3.18	3.20	3.40	3.83	3.68
Total	100.08	99.59	99.54	99.89	99.87

Cations based on 8 oxygens

Sample #	102	102	131	131	131
Si	8.23	8.21	8.61	8.57	8.59
Al	4.18	4.18	3.88	3.89	3.88
Mg					
Ca	1.27	1.30	0.80	0.90	0.87
Fe*	0.02	0.01	0.02	0.02	0.03
Na	2.36	2.40	2.77	2.93	2.78
K	0.40	0.39	0.39	0.26	0.36
Cl	0.81	0.82	0.86	0.98	0.94
Total	17.27	17.32	17.33	17.55	17.45

* Indicates Total iron as Fe+2

Analyses 1 and 2 are from sample 102; analyses 3, 4, and 5 are from sample131.

Table 9. Compilation of stratigraphic thicknesses for overburden at the time of metamorphism and correlation to pressure conditions.

Stratigraphic Unit	Geologic Age	Minimum Thickness (ft)	Maximum Thickness (ft)	Reference(s)
Andesite-Dacite	Tertiary	300	1000	Balk (1962); Leonard (1982)
Older Rhyolite	Tertiary	775	775	Leonard (1982)
Cretaceous Sediments	Cretaceous	1000	1540	Balk (1962); Griswold (1961)
Hueco Formation	Permian	360	525	Balk (1962); Griswold (1961)
Pennsylvanian Undivided	Pennsylvanian	350	636	Balk (1962); Griswold (1961)
Total (ft)		2785	4476	
Total (km) (3280.84ft/km)		0.85	1.4	
Pressure (265kbar/km)		225	371	

Table 10. Bulk composition of the matrix in sample TH12S-112. See Appendix 6 for the calculation.

Bulk Composition of TH12S-112	
SiO2	48.780
TiO2	0.747
Al2O3	16.742
Cr2O3	0.001
MgO	1.066
CaO	29.749
MnO	0.102
FeO	1.484
Na2O	0.984
K2O	0.033
Total	99.686

APPENDICES

Appendix 1. Field Area Access Map

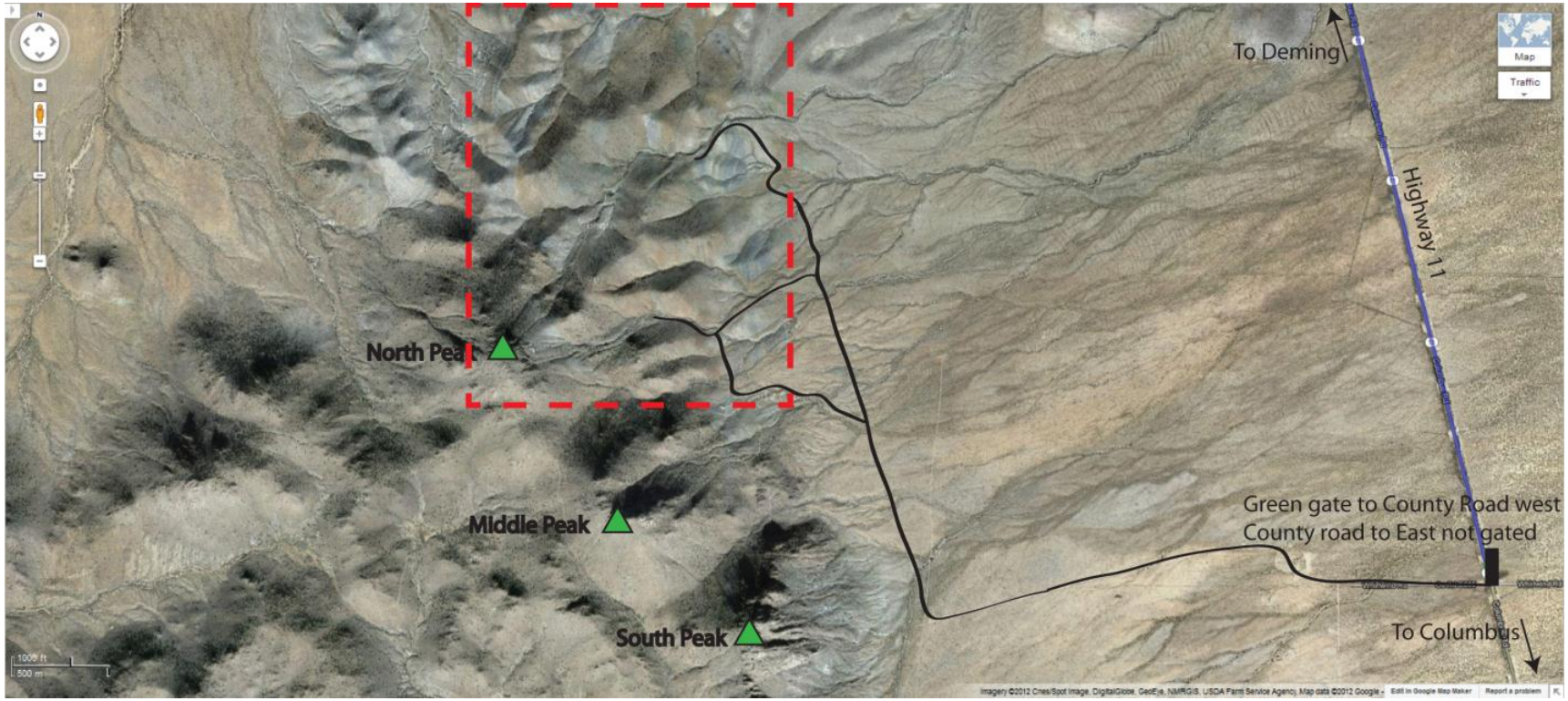

Map demonstrating BLM land roads that access the field area. These roads are not maintained past the couple residents who live near the road and may be washed out. Image taken from google maps.

Gate to County Road B005, Whirlwond Road, at intersection with NM Highway 11 looking west to the Tres Hermanas Range (south peak on the left and North Peak to the right). The gate is not locked.

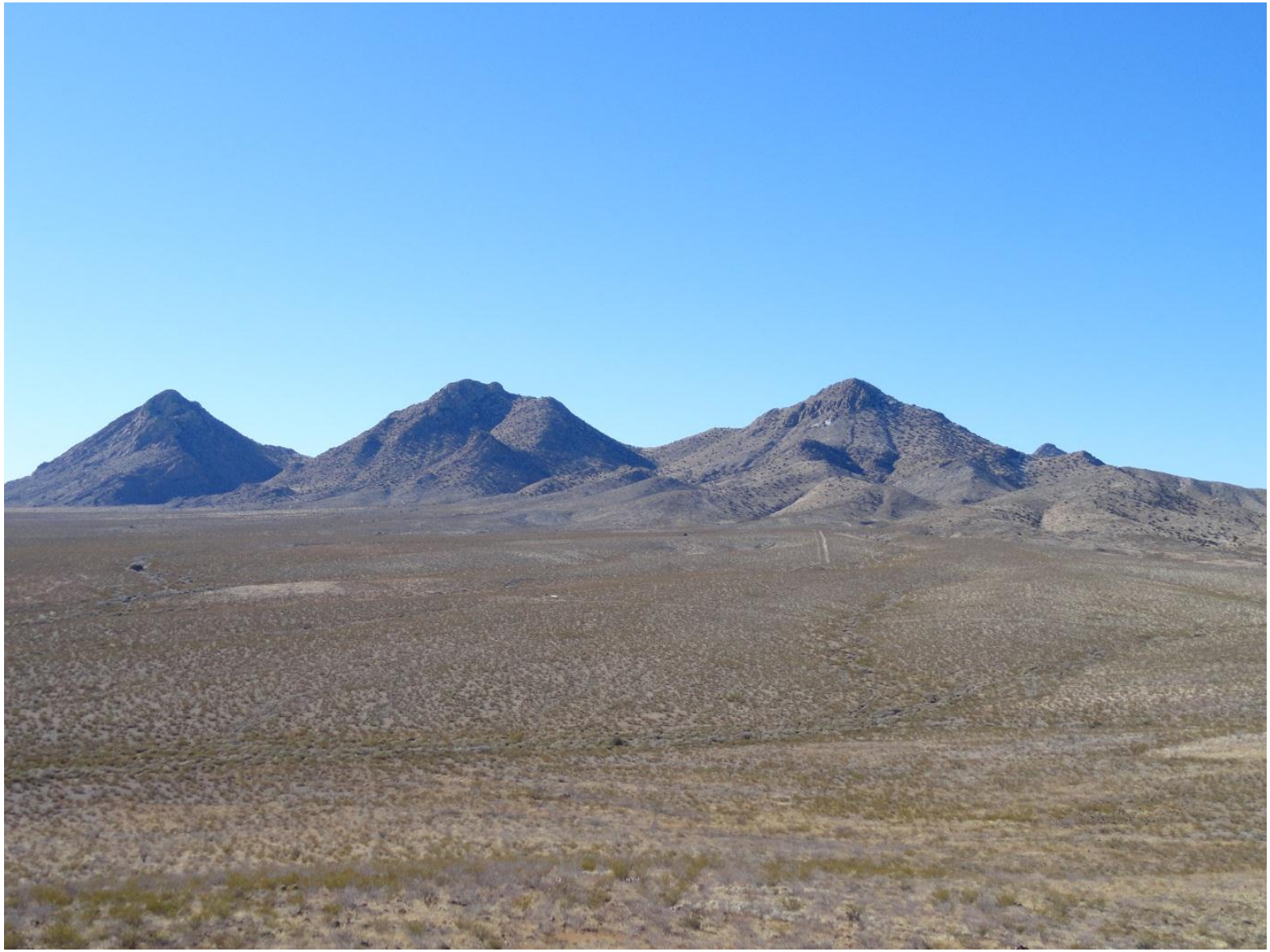

View of South Peak (left), Middle Peak, and North Peak (right) as viewed from Greasewood Hills near NM Highway 11 looking to the southwest.

Appendix 2. Phase Data tables.

This is a digital file titled Snyder_Appendix_2_Assemblages.xlsx

Appendix 3. Electron probe microanalyses.

This is a digital masterfile of analyses titled Snyder_Appendix_3_EPMA_Results.xlsx.

Appendix 4. ArcGIS Database and Field Data.

This file includes the North Peak quadrangle, Hillshade DRG, Snyder waypoint shapefiles, Anovitz Sample Shapefile, county shapefile, and state shapefile.

Appendix 5. THERMOCALC calculations.

This file contains the THERMOCALC output files for the calculations that were used in this study including those used to make the P-T and T-X graphs. The file is titled Snyder_Appendix_5_THERMOCALC_output.docx.

VITA

Carissa D. Snyder was born January 26, 1988 to Melinda M. and Conrad E. Snyder in DuBois, Pennsylvania. After finishing her primary education in the Punxsutawney Area School District in 2006, she attended Bloomsburg University of Pennsylvania, in Bloomsburg, PA. She obtained her B.S. in Geology with a minor in Geography August 2010. She then pursued a Master's of Science degree at the University of Tennessee in Knoxville, TN.